STUDY OF THE MECHANO-CHEMICAL REGULATION IN ACTIN DEPOLYMERIZATION KINETICS

A Dissertation
Presented to
The Academic Faculty

by

Cho-yin Lee

In Partial Fulfillment
of the Requirements for the Degree
Doctor of Philosophy in the
School of Biomedical Engineering

Georgia Institute of Technology
August 2010

STUDY OF THE MECHANO-CHEMICAL REGULATION IN ACTIN DEPOLYMERIZATION KINETICS

Approved by:

Dr. Larry V. McIntire, Advisor
Wallace H. Coulter Department of Biomedical Engineering
Georgia Institute of Technology and Emory University School of Medicine

Dr. Suzanne G. Eskin
Wallace H. Coulter Department of Biomedical Engineering
Georgia Institute of Technology and Emory University School of Medicine

Dr. Shoichiro Ono
Department of Pathology and Laboratory Medicine
Emory University School of Medicine

Dr. Raymond P. Vito
Wallace H. Coulter Department of Biomedical Engineering
Georgia Institute of Technology and Emory University School of Medicine

Dr. Cheng Zhu
Wallace H. Coulter Department of Biomedical Engineering
Georgia Institute of Technology and Emory University School of Medicine

Date Approved: May 11, 2010

To my dearest family.

ACKNOWLEDGEMENTS

I wish to express my deep gratitude to many people who have given me support and guidance for the work described in this dissertation. I would first like to thank my advisor Dr. Larry McIntire and Dr. Suzanne Eskin for creating a supportive and liberal research environment which has encouraged my creativity and imagination in science. I also appreciate their knowledge and wisdom guiding me though every challenge and difficulty happening during my Ph.D. study.

I deeply appreciate the invaluable contribution from the collaborators of this project and the rest of my thesis committee. In particular I wish to thank Dr. Cheng Zhu and Dr. Shoichiro Ono for their enthusiastic advice with constant patience, support with the resources of their labs, and constructive debate and brain storm encouraging me to think deeper and further. I also wish to thank Dr. Jizhong Lou, a friend and a fellow colleague, for his elegant works in SMD simulations. In addition I want to thank Dr. Peter Rubenstein and Dr. Kuo-Kaung Wen, for their timely support and joining in with yeast actin mutants, enabling the project to go in depth. Finally I want to thank Dr. Raymond Vito. It's a great honor of mine to have him on my thesis committee. The collaborative efforts from them have been pushing this work from good to great.

I want to thank my fellow colleagues in Dr. McIntire's lab and Dr. Zhu's lab, particularly Dr. Daniel Conway, Dr. Fang Kong, Jianggou Lin, Dr. Jin Qian, Yumiko Sakurai, and Xue Xiang, for their technical support, helpful discussions and friendship.

I would also like to thank the National Science Coucil, Ministry of Education and the Council of Economic Planning & Development of The Republic of China (Taiwan), for enrolling me into the Taiwan Merit Scholarship program, which encourages scholastically outstanding Taiwanese to pursue advanced studies at prestigious academic institutions overseas.

Last but not the least, I wish to express my deepest gratitude to my family. Thank you to my parents, whose love has constantly supported me for thirty years to this step, and my wife, for her companionship throughout every challenge and adventure in the future of my life.

TABLE OF CONTENTS

LIST OF FIGURES

LIST OF ABBREVIATIONS

ACTA1	The gene encoding human alpha skeletal muscle actin
AFM	Atomic force microscopy
ADP	Adenosine diphosphate
Arg	Arginine (also R), an amino acid
Asp	Aspartic acid (also D), an amino acid
ATP	Adenosine triphosphate
BAECs	Bovine aortic endothelial cells
BSA	Bovine serum albumin
D	Aspartic acid (also Asp), an amino acid
DAD	diaphanous auto-regulatory domain
DID	diaphanous inhibitory domain
E	Glutamic acid (also Glu), an amino acid
E195S	Actin mutant with Glutamic acid replaced by Serine at the position 195
F-actin	Actin polymer or actin filament
FH1	formin homology domain 1
FH2	formin homology domain 2
G	Glycine (also Gly), an amino acid
G-actin	Actin monomer
GDP	Guanosine diphosphate
Gln	Glutamine (also Q), an amino acid
Glu	Glutamic acid (also E), an amino acid

Gly	Glycine (also G), an amino acid
GTPγS	Guanosine gamma thio-phosphate, a non-hydrolyzable GTP analog
K	Lysine (also Lys), an amino acid
K113S	Actin mutant with Lysine replaced by Serine at the position 113
Lys	Lysine (also K), an amino acid
mDia1 C-t	C-terminal construct of mDia1 protein
mDia1 N-t	N-terminal construct of mDia1 protein
NM	Nemaline myopathy
PBS	Phosphate buffered saline
PZT	Piezoelectric translator
Q	Glutamine (also Gln), an amino acid
R	Arginine (also Arg), an amino acid
S	Serine (also Ser), an amino acid
Ser	Serine (also S), an amino acid
SMD	Steered molecular dynamics
TFZ	Tension free zone
WT	Wild type

SUMMARY

A fundamental yet unresolved issue in cell biology is how force regulates actin dynamics and how this biophysical regulation is modulated by biochemical signaling molecules. Here we show, by atomic force microscopy (AFM) force-clamp experiments, that tensile force regulates the kinetics of G-actin/G-actin and G-actin/F-actin interactions by decelerating dissociation at low forces (catch bonds) and accelerating dissociation at high forces (slip bonds). The catch bonds can be structurally explained by force-induced formation of new interactions between actin subunits (Steered molecular dynamics (SMD) simulations performed by Dr. Jizhong Lou, Institute of Biophysics, Chinese Academy of Sciences, Beijing, China). K113S mutation on yeast actin suppressed the actin catch-slip bonds, supporting the structural mechanism proposed by SMD simulations. Moreover, formin controlled by a RhoA-mediated auto-inhibitory module can serve as a "molecular switch", converting the catch-slip bonds to slip-only. These results imply anisotropic stability of the actin network in cells subjected to directional forces, possibly explaining force-induced cell and actin fiber alignment controlled by RhoA and formin. Our study suggests a molecular level crosstalk mechanism bridging the actin-mediated mechanotransduction and biochemical signal transduction pathways.

CHAPTER 1: THESIS RATIONAL

1.1 Introduction

Actin monomer, or G-actin, is an intracellular globular-shaped protein with a molecular weight of about 43 kDa (Kabsch et al., 1990). It is the most abundant protein in eykaryotic cells and highly conserved throughout evolution; there is 80% conservation at the gene level between human and yeast, and 95% conservation of the protein primary structure (Alberts et al., 2002; Howard, 2001). Actin filament, or F-actin, is the polymer of actin. It is a double-stranded right-handed helix assembled from actin monomers through weak non-covalent interactions (Alberts et al., 2002; Holmes et al., 1990; Howard, 2001). Because the actin monomers are asymmetrical, the ends of the actin filament are structurally different. The more dynamic end with faster on rate and off rate (higher k_{on} and k_{off}) is called the plus (+) or the barbed-end, whereas the other end is called the minus (-) or the pointed-end (Pollard and Borisy, 2003). F-actin filament is the major component of actin cytoskeleton, which primarily works as a force bearing and generating structure in eukaryotic cells (Fletcher and Mullins, 2010) (Fig. 1).

The growing of actin filaments is undergoing dynamic polymerization processes, starting from the nucleation of its monomer subunits. During the growing process of the F-actin, actin momoner subunits are coming on and off at the ends of the filament. The buffer with high salt concentration, or F-buffer, favors the filament formation, while the low-salt buffer, or G-buffer, makes the actin to stay in its monomer form (Alberts et al., 2002; Howard, 2001).

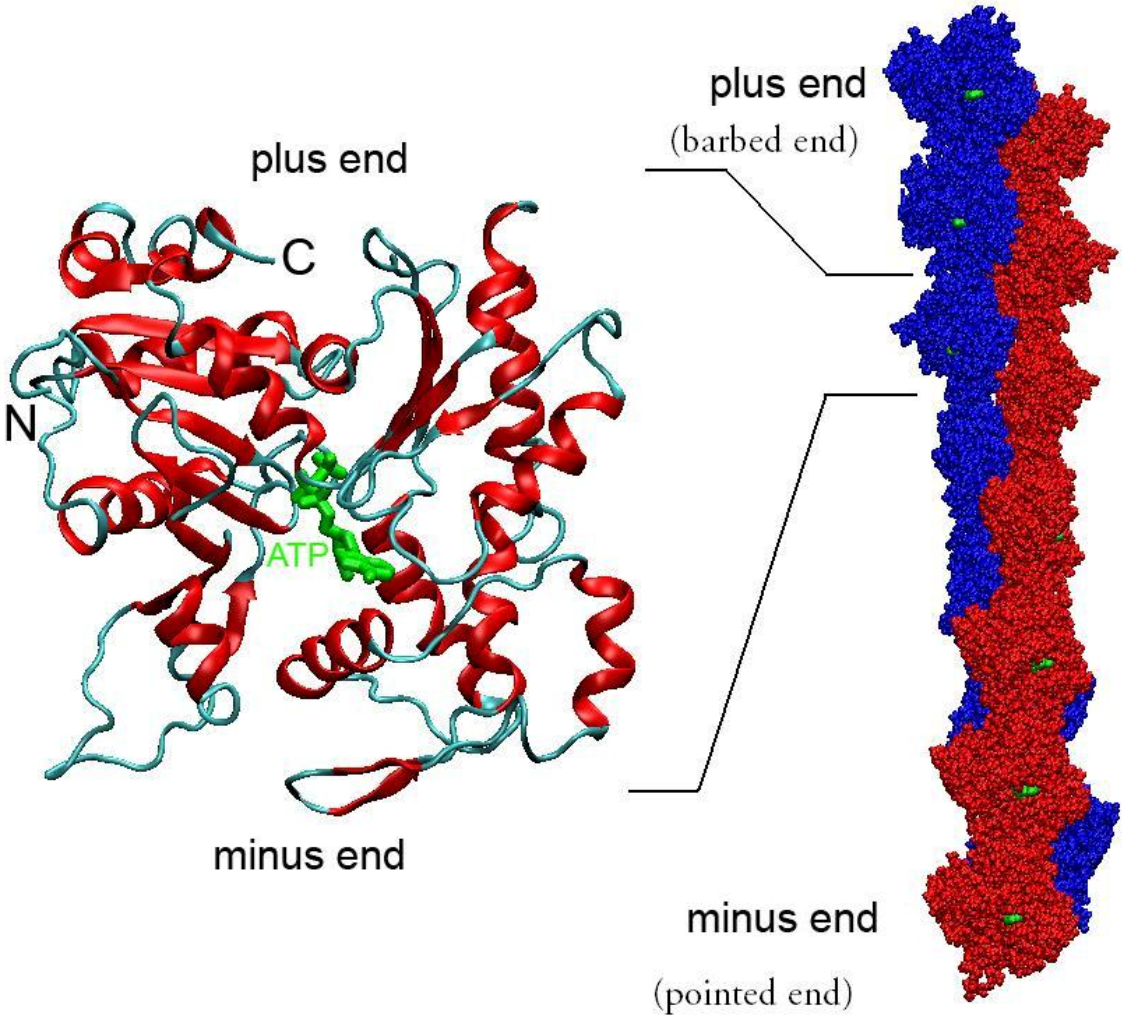

Figure 1. The structure and organization of G-actin and F-actin. The asymmetrical globular-shaped G-actin *(Left)* is the monomer subunit of the double-stranded right-handed F-actin polymer *(right)*, which has a plus end (barbed end) and a minus end (pointed end). Adapted and modified from (Alberts et al., 2002).

In cells, the dynamic polymerization of actin filaments enables the dynamic rearrangement of actin cytoskeleton. The actin cytoskeleton at one site of the cell can disassemble into small soluble subunit, then diffuse to and re-assemble into new actin cytoskeletal structure at the new site of the cell (Alberts et al., 2002). This dynamic reorganization of actin cytoskeleton controls many important cell processes, such as cell

shape, orientation, motility and cytokinesis (Kaunas et al., 2005; Pollard and Borisy, 2003; Pollard and Cooper, 2009).

In vivo, the dynamic reorganization of the actin cytoskeleton is controlled by extracellular physiological forces, as it is crucial to mechanotransduction and cellular adaptations to mechanical stresses (Chien, 2007; del Alamo et al., 2008; Hirata et al., 2008; Kaunas et al., 2005; McCue et al., 2004; Sung et al., 2007). This dynamic process is also controlled by intracellular biochemical signaling such as Rho-related GTPase pathways. Rho, Rac and Cdc42 induce the assembly of actin stress fibers, lamellipodia, and filopodia respectively *in vivo* (Etienne-Manneville and Hall, 2002; Hall, 1998; Hall and Nobes, 2000; Maekawa et al., 1999; Narumiya et al., 1997; Nobes and Hall, 1995).

Among biochemical regulators of actin dynamics, RhoA, which is considered a molecular switch (Hall and Nobes, 2000), controls the activity of formin which directly participates in actin filament assembly. By stabilizing actin nuclei (Li and Higgs, 2003; Pring et al., 2003; Zigmond, 2004) and continuously binding to the barbed ends of actin filaments (Otomo et al., 2005; Xu et al., 2004), the highly conserved active formin homology domain FH2 alters actin dynamics through accelerating nucleation and stabilizing barbed-end elongation (Higgs, 2005; Kovar, 2006; Paul and Pollard, 2009) (Fig. 2A). In mDia1, a mammalian formin, the FH2 domain is auto-inhibited by the interaction between the N-terminal diaphanous inhibitory domain (DID) and the C-terminal diaphanous auto-regulatory domain (DAD). Binding of RhoA to the N-terminus relieves the DAD-DID auto-inhibition (Higgs, 2005; Li and Higgs, 2003) (Fig. 2B).

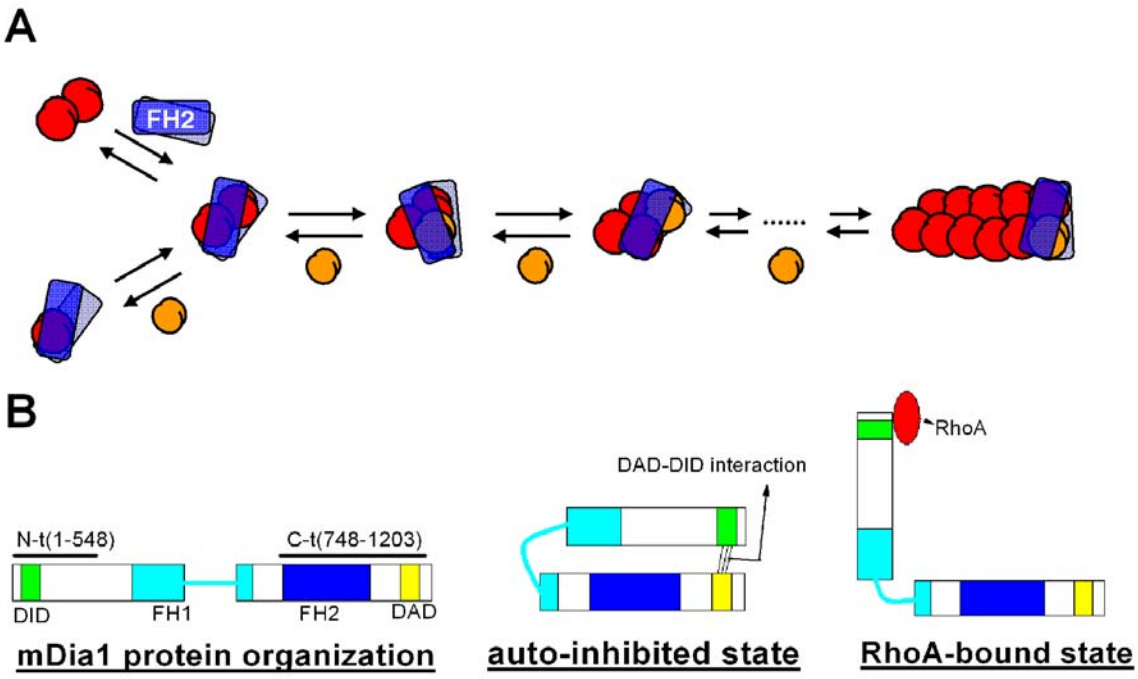

Figure 2. The function and regulation of formin. (A) The FH2 domain of formin stabilizes actin nuclei (red) and continuously binds to the barbed end of actin filaments while allowing the addition of new actin monomer (orange) to the barbed end. (modified from Zigmond, 2004) (B) Organization and regulation of mDia1 protein domains. Lines above the diagram represent constructs used in this study: mDia1 N-t and mDia1 C-t, with the starting and ending amino acids specified. The active FH2 domain is auto-inhibited by the DAD-DID interaction, which is relieved when RhoA binds to the N-terminus to compete with DAD. Adapted and modified from (Higgs, 2005).

Remarkably, extracellular forces and intracellular biochemical signaling work cooperatively to control actin dynamics. Signaling molecules can influence the way force regulates actin dynamics *in vivo*. For example, the alignment of the cell and its actin stress fibers in response to unidirectional periodic stretch is switched by RhoA through mDia1. This alignment is perpendicular to the stretch direction when RhoA and mDia1 are involved, and parallel to the stretch direction if RhoA or mDia1 is compromised (Kaunas et al., 2005) (Fig. 3).

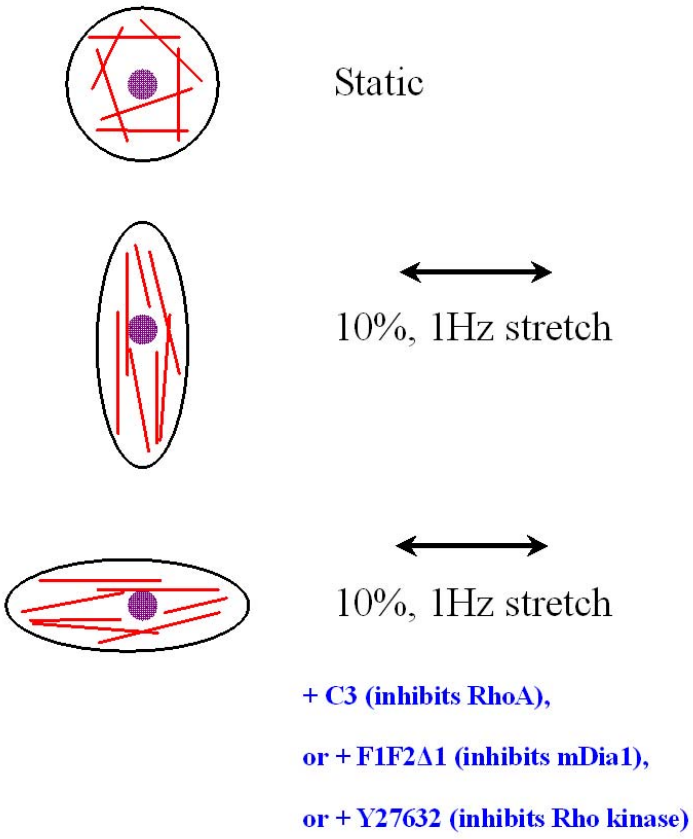

Figure 3. Effects of inhibition of RhoA, mDia and Rho kinase on the stretch-induced stress fiber orientation in cells. The stretch-induced actin stress fiber (red lines) orientation is perpendicular to the stretch direction in control conditions. It is parallel to the stretch direction if RhoA, mDia1, or Rho kinase is inhibited by C3, F1F2Δ1, or Y27632, respectively (Kaunas et al., 2005).

These observations motivated us to pursue the molecular-level mechanistic details explaining how actin dynamics are regulated by force and how this regulatory pattern is further modulated by biochemical molecules. This issue is crucial to illuminate the crosstalk between the actin-mediated mechanotransduction and biochemical signal transduction pathways, and to understand the cellular adaptations of morphological changes under physiological force stimuli. Here we used AFM force-clamp experiments to elucidate how force regulates the dissociation kinetics of the G-actin/G-actin and G-

actin/F-actin interactions, and dissected the effect of RhoA and formin on this kinetics-force relationship.

1.2 Specific Aims

1.2.1 Specific Aim I: Measure the force-dependent bond lifetimes of G-actin/G-actin interactions.

It is hypothesized that the G-actin/G-actin interactions are regulated by force via catch bonds, where the tether force decelerates the dissociation of two interacting molecules, over the force range relevant to the force-bearing function of a single actin filament *in vivo*. This hypothesis implies that the actin network is the most stable in the direction of the maximal stress in the stress field applied, which is in line with previous *in vivo* study showing that the cell and its actin stress fibers aligns parallel to the applied periodic uni-axial stretch when RhoA or formin is inhibited thus not involved (Kaunas et al., 2005) (Fig. 3).

To test the hypothesis, we used AFM force-clamped experiments to measure the bond lifetimes of G-actin/G-actin interactions under different magnitudes of clamped tether force.

1.2.2 Specific Aim II: Measure the force-dependent bond lifetimes of G-actin/F-actin interactions.

The actin filament in the cytoskeleton is the functional unit bearing tensile force in cells. It is polymerized from its G-actin subunits, and is viewed as a two-stranded,

right-handed helix because there is extensive monomer-monomer contact between alternate monomers, and the rotation per monomer is large (166^{o}) (Holmes et al., 1990).

Depolymerization of the terminal actin subunit from the filament tip involves dissociation of two G-actin/G-actin bonds (intra-strand; long-pitch and inter-strand; short-pitch) arranged in parallel (Holmes et al., 1990; Howard, 2001). Therefore it is hypothesized that G-actin/F-actin interactions are also regulated by tensile force via a catch-bond mechanism, according to the similar reasoning mentioned in Specific Aim II.

As in the study of G-actin/G-actin interactions, we used AFM force-clamped experiments to measure the force-dependent bond lifetimes of G-actin/F-actin interactions. Considering the polarity of F-actin, we isolated the activity of a specific single end in G-actin/F-actin measurements by introducing CapZ, which tightly blocks the actin dynamics at the barbed-end (Zigmond et al., 2003), and/or Tmod3, which inhibits the activity at the pointed-end (Babcock and Fowler, 1994; Fischer et al., 2003).

1.2.3 Specific Aim III: Characterize the regulation of the RhoA/formin autoinhibition module to the force-dependent bond lifetimes of actin subunit interactions.

It has been shown that when the cell and its actin stress fibers aligns perpendicular to the direction of the applied periodic uni-axial stretch when RhoA and formin are involved (Kaunas et al., 2005)(Fig. 3). This implies that the actin network is the most stable in the direction of the minimal stress in the stress field applied. Therefore it is hypothesized that in the presence of FH2 domain of formin, the functional active unit of the RhoA/fromin module, force regulates actin subunit interactions by accelerating the

dissociation of interacting actins (slip-bonds), over the force range relevant to the force-bearing function of a single actin filament *in vivo*.

Besides, it is hypothesized that the activity of FH2 domain on the force-regulated actin dissociation kinetics is controlled by a RhoA mediated DAD-DID auto-inhibitory module, as previously described (Higgs, 2005; Li and Higgs, 2003) (Fig. 2B).

To test these hypotheses, we used AFM force-clamped experiments to measure the force-dependent bond lifetimes of G-actin/G-actin and G-actin/F-actin interactions as mentioned in Specific Aim I and II, in the presence the mDia1 C-t, an mDia1 C-terminal construct containing FH2 and DAD domains. We then test the effect of DAD-DID auto-inhibition by adding the DID domain-containing N-terminal construct of mDia1 (mDia1 N-t) into the AFM assay system, and test the relieving effect of RhoA on the DAD-DID autoinhibition (Fig. 2B).

CHAPTER 2: MATERIALS AND METHODS

2.1 Proteins

Biotinylated rabbit skeletal muscle G-actin (Cat: AB07, covalently linked with biotin at random surface lysine residues, approximately 1 biotin per actin monomer) and Pyrene-labeled rabbit skeletal muscle G-actin was from Cytoskeleton Inc. (Denver, CO). Latrunculin A was from Sigma Aldrich (St. Louis, MO). Chicken CapZ was expressed in *E.coli* and purified by Dr. Shoichiro Ono's lab as described (Soeno et al., 1998). Budding yeast formin construct Bni1p(FH1FH2)p containing FH1 and FH2 domains but without the inhibitory domain was a gift from Dr. David Kovar (University of Chicago) (Kovar and Pollard, 2004). Biotinylated wild type yeast actin and biotinylated yeast actin mutant K113S was provided by Dr. Peter A Rubenstein (University of Iowa).

Mouse formin mDia1 constructs (N-terminal: 1-548, C-terminal: 748-1203) in pGex-KT, provided by Dr. Henry N. Higgs (Dartmouth Medical School) were expressed and purified as described previously (Li and Higgs, 2003, 2005). They were expressed in Rosetta2 E.coli (Novagen) which were then grown to OD600 0.6-0.8 in LB with 100ug/ml ampicillin and 34 ug/ml chloramphenical at 37C. The cultures were then cooled down to 16C, added 0.5mM IPTG and grown overnight. After centrifuging, the pelleted bacteria were resuspended in EB(50mM Tris-HCl pH 8, 500mM NaCl, 5mM EDTA, 1mM DTT and 1 pill/50ml complete protease inhibitor [Roche]) then sonicated. After ultracentrifugation, supernatant added with 0.1% Thesit was loaded onto

glutathione-sepharose 4B (GE-healthcare) equilibrated with WB (5mM Tris-HCl pH 8, 250mM NaCl, 0.05mM EDTA, 1mM DTT and 0.1% Thesit) then washed extensively with WB. The mixture with 50% slurry of beads was then added with 10U/ml thrombin (Amersham) and mixed for 2 hrs at 4C. After the cleaved protein was drained from the column, thrombin was inactivated by 1mM PMSF for 15 minutes, after which DTT was added to a concentration of 10mM. Both N-terminal and C-terminal constructs were dialyzed against the following buffer: 2mM NaPO4, pH 7.0, 150 NaCl, 0.1mM EGTA, 0.5mM DTT. mDia1 proteins were stored at 5μM at -20 ^{o}C with 50% glycerol to avoid loss of activity upon freezing(Li and Higgs, 2005).

Human tropomodulin Tmod3 construct in pGex-KG, provided by Dr. Velia M. Fowler (Scripps Research Institute) was expressed and purified as described previously (Babcock and Fowler, 1994; Fischer et al., 2003). It was expressed in Rosetta2 E.coli (Novagen) which were then grown to OD600 0.6-0.8 in LB with 100ug/ml ampicillin and 34 ug/ml chloramphenical at 37C. The cultures were then cooled down to 25C, added 0.5mM IPTG and grown for 3hours. After centrifuging, the pelleted bacteria were resuspended in EB (PBS and 2mM DTT and 1 pill/50ml complete protease inhibitor [Roche]) then sonicated. 0.1% polyethylenimine was added to the sonicated extract. After ultracentrifugation, supernatant was loaded onto glutathione-sepharose 4B (GE-healthcare) equilibrated with WB (20mM Tris-HCl pH 8, 150mM NaCl, 2.5mM $CaCl_2$, and 1mM DTT) then washed extensively with WB. The mixture with 50% slurry of beads was then added with 5U/ml thrombin (Amersham) and mixed for 2 hrs at 4C. After the cleaved protein was drained from the column, thrombin was inactivated by 2mM

PMSF for 15 minutes, after which the sample was dialyzed against the following buffer: 5 mM Tris-HCl pH 8.0, 0.2 mM $CaCl_2$, 0.5 mM DTT, 50 mM KCl, and 2 mM $MgCl_2$.

The concentrations of purified mDia1 and Tmod3 constructs were determined by densitometry of Coomassie blue-stained gels after SDS-PAGE using known amounts of actin as standards. His-RhoA (Cytoskeleton) was charged with GTPγS (Cytoskeleton) or GDP (Roche, Nutley, NJ) as described previously (Higgs and Pollard, 2000; Watanabe et al., 1999). 100μM His-RhoA was mixed with 6.66 mM GTPγS or GDP in the following buffer: 50 mM Tris-HCl pH 7.5, 0.5 mM $MgCl_2$, 50 mM NaCl, 0.5% sucrose, 0.1% dextran, 1 mM DTT and 5mM EDTA. The mixture was incubated at room temperature for 15 min, supplemented with $MgCl_2$ to a final concentration of 10 mM, then kept on ice and used within 2 hr.

2.2 Measuring the bond lifetimes-force relationship by AFM

2.2.1 AFM setup

Our custom-made AFM and force-clamped experimental procedures for measuring lifetimes of single bonds have been previously described (Kong et al., 2009; Marshall et al., 2003; Yago et al., 2008). The AFM consisted of a piezoelectric translator (PZT) (Physik Instrument, Karlsruhe, Germany) on which a cantilever (Vecco, Plainview, NY) was mounted. The deflection of the cantilever was detected by a photodiode sensing the displacement of a laser beam (Oz optics, Ontario, Canada) focused on then reflected from the cantilever tip (Fig. 4).

The cantilever deflection was converted to the magnitude of the causing force according to spring constants (2-20pN/nm) of the cantilever, which were calibrated during each experiment using thermal fluctuations analysis (Wu et al., 2005).

A computer (Dell, Round Rock, TX) with a data acquisition board (PCI-MIO-16XE-10, National Instruments, Austin, TX) controlled the movement of the PZT and received the signal input from the pre-amplification circuit board coupling the photodiode.

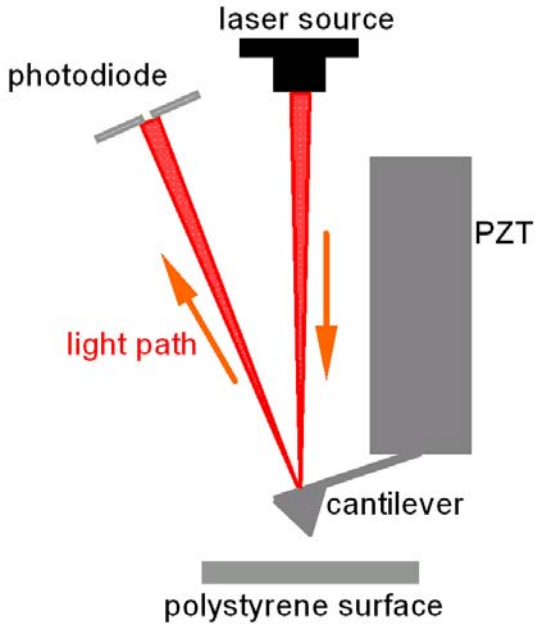

Figure 4. The AFM schematic.

2.2.2 Functionalizing AFM probes with actin molecules

To functionalize the AFM probes for G-actin/G-actin interactions (Fig. 5, *left*), the cantilever tip and the polystyrene dish surface were incubated with 2 mg/ml biotinylated BSA (Sigma Aldrich) at 4 ^{o}C overnight, washed 3 times with PBS, incubated

with 1 mg/ml streptavidin (Sigma Aldrich) for 1 hr at room temperature, washed 3 times with G-buffer (5 mM Tris-HCl pH 8.0, 0.2 mM $CaCl_2$, 0.2 mM ATP, 0.5 mM DTT), and incubated at 4 ^oC for 1 hr with 1μM biotinylated G-actin in G-buffer containing 0.00025% biotin to achieve low G-actin coating density required for single-bond measurements. For G-actin/F-actin interactions (Fig. 5, *right*), the cantilever tip was functionalized by the same way as that for G-actin/G-actin interactions, but the polystyrene surface was functionalized with sonicated F-actin instead of actin monomer. To prepare the sonicated F-actin, 4μM of G-actin (biotinylated actin: non-labeled actin = 1:20 unless otherwise stated) was incubated in F-buffer (G-buffer + 50 mM KCl, 2 mM $MgCl_2$, 1 mM ATP) for 15 minutes at room temperature, then sonicated for 1 minute (5 seconds on, 5 seconds off), followed by 2 more cycles of 15-minute incubation + 1-minute sonication (Branson 1510 from Branson, Danbury, CT). After the last sonication, the F-actin was immediately applied to the biotin/streptavidin-treated polystyrene surface with 0.00025% biotin. To measure interactions between actins, the G-buffer was replaced with F-buffer (G-buffer + 50 mM KCl, 2 mM $MgCl_2$, 1 mM ATP) containing 0.00025% biotin to block any non-saturated binding-sites of streptavidin in the presence or absence of indicated concentrations of His-RhoA and/or formin constructs. In specificity control experiments, the conditions were changed to: 1) replacing the biotinylated G-actin on the cantilever with biotinylated BSA, after incubating the cantilever with biotinylated BSA and streptavidin; 2) replacing F-buffer with G-buffer as working solution; or 3) adding 100μM latrunculin A to the working buffer. To measure biotin/streptavidin interactions, only the polystyrene surface was further incubated with streptavidin after adsorption with

biotinylated BSA. The working solution for biotin/streptavidin interactions was F-buffer without soluble biotin (Fig. 5, *middle*).

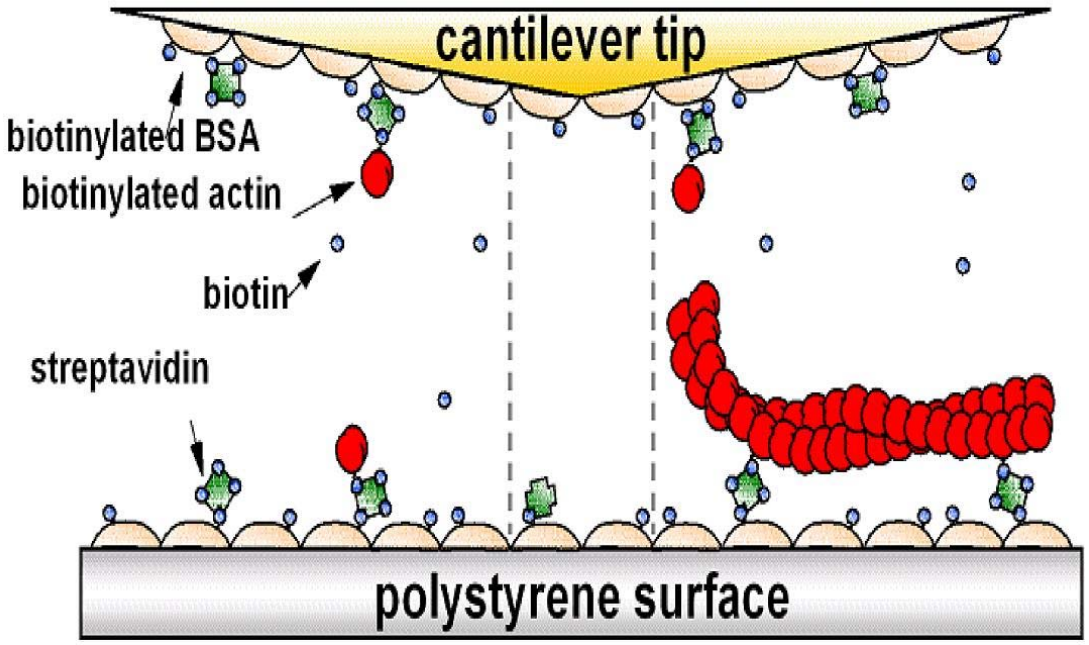

Figure 5. Functionalizing AFM probes. AFM cantilever tip and polystyrene surface functionalized for G-actin/G-actin (*left*), biotin/streptavidin (*middle*) or G-actin/F-actin (*right*) interactions. Actin (red), biotin (blue), steptavidin (green) and BSA (beige) are depicted.

2.2.3 Measurement of the bond lifetimes-force relation

A force-clamp program involving a feedback system written in LABVIEW (National Instruments, Austin, TX) was used to control the whole module for bond lifetimes measurement. During each measurement cycle, one probe, cantilever tip coated with actin molecules, was driven into contact with another probe, polystyrene surface coated with actin molecules, at 200nm/s, then was retracted to 0-5nm above the surface, held for 0.5 second to allow the bond formation, and was retracted further at the same speed. Once a binding event was detected during the retraction, the program clamped the

tether force at the preset level to measure the bond lifetime under the given loading force. The binding frequency was kept low (<25%) to ensure that most binding happens as a single bond. Only single-step dissociations were analyzed. Each data point presented to illustrate the lifetime-force relationship is an average of 50-200 analyzed measurements at a given force bin.

2.3 Actin polymerization assay

Pyrene-labeled G-actin was prepared in 1uM stock with G-buffer. Polymerization was induced by adding 10X F-buffer to a concentration of 1X, with or without mDia1 constructs and/or His-RhoA. Added proteins were mixed together for 1 minute prior to their rapid addition to Pyrene-labeled G-actin stock to start the assay. Pyrene fluorescence was monitered by VICTOR3 1420 Multilabel Counter (Perkin Elmer Life Science), with an excitation filter 355/40m and an emission filter 430/20m, both from Chroma Tehcnology Corp. The time between the mixing of final components and the start of fluorescence data collection was monitered and controlled to be in a range of 5 to 10 seconds.

CHAPTER 3: RESULTS

3.1 System validation

To study how force regulates actin kinetics at the single-bond level, G-actin monomers were immobilized on the AFM cantilever tip via a biotin-streptavidin coupling (Fig. 5). The polystyrene surface was functionalized with G-actin monomers or F-actin filaments via a biotin-streptavidin system for studying of G-actin/G-actin (Fig. 5, *left*) or G-actin/F-actin (Fig. 5, *right*) interactions, respectively. The functionalized tip was driven into contact with the functionalized surface, retracted, and clamped at a constant force to pull on the bond formed during contact. The bond lifetime at that force was then measured (Fig. 6).

A tension-free zone (TFZ) was characteristic of the force-scan traces of G-actin/F-actin interactions (Fig. 6, *right*), but not in G-actin/G-actin interactions (Fig. 6, *left*) or in non-specific binding controls. A TFZ has been demonstrated in AFM measurements of interactions between lengthy molecules because they need to be picked up and fully extended before they can resist any tensile forces (Marshall et al., 2006). In Fig. 6 the TFZ is interpreted as a period during which the G-actin/F-actin bond is formed but the F-actin filament is not fully stretched between the retracting cantilever tip and the biotin/streptavidin anchoring site on the filament. The TFZ is terminated by detecting a tether force on the G-actin/F-actin bond due to full stretching of a segment of filament between the cantilever tip and the biotin/streptavidin anchoring site nearest to the filament end. This interpretation of TFZ is supported by that the length distribution of

TFZ is left-shifted when the ratio of biotinylated actin/unlabeled actin in the F-actin tested was increased to shorten the average length of a F-actin segment free of biotinylated actin (Fig. 7).

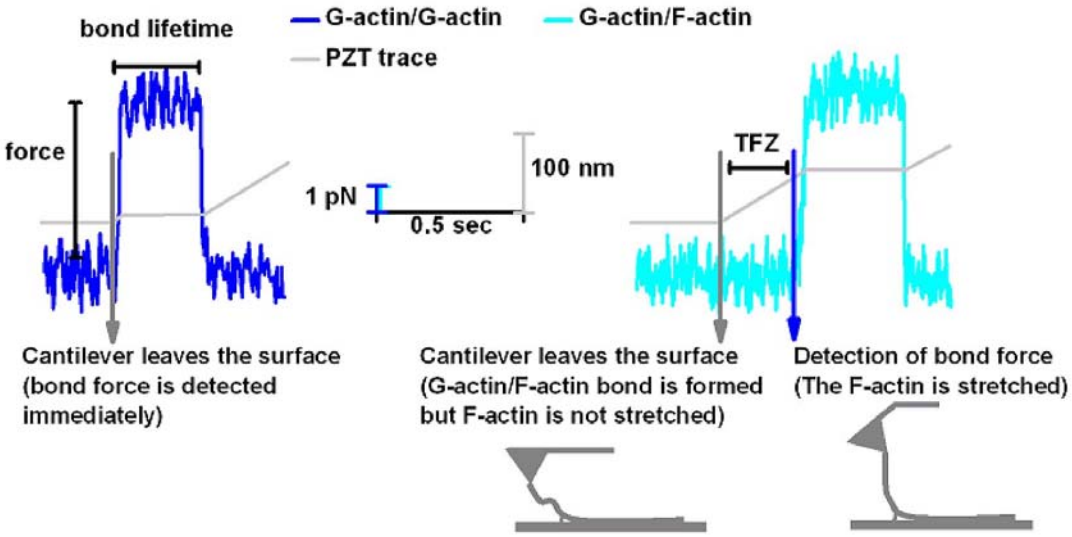

Figure 6. Representative force-scan trace for G-actin/G-actin and G-actin/F-actin interactions illustrating the bond lifetime measured at a given force. Trace for the movement of the piezoelectric translator (PZT) is depicted in gray. The PZT retracted then held the cantilever tip at a given distance from the surface, applying tensile force on the bond. Bond rupture reset the force trace to the baseline. In G-actin/F-actin interactions (cyan, *right*), a tension-free zone (TFZ) was defined as the period between the onset of PZT retraction and detection of a bond force. Retracting the cantilever tip through the tension-free zone (TFZ) did not apply tensile force to the bond, until the F-actin was fully extended and stretched.

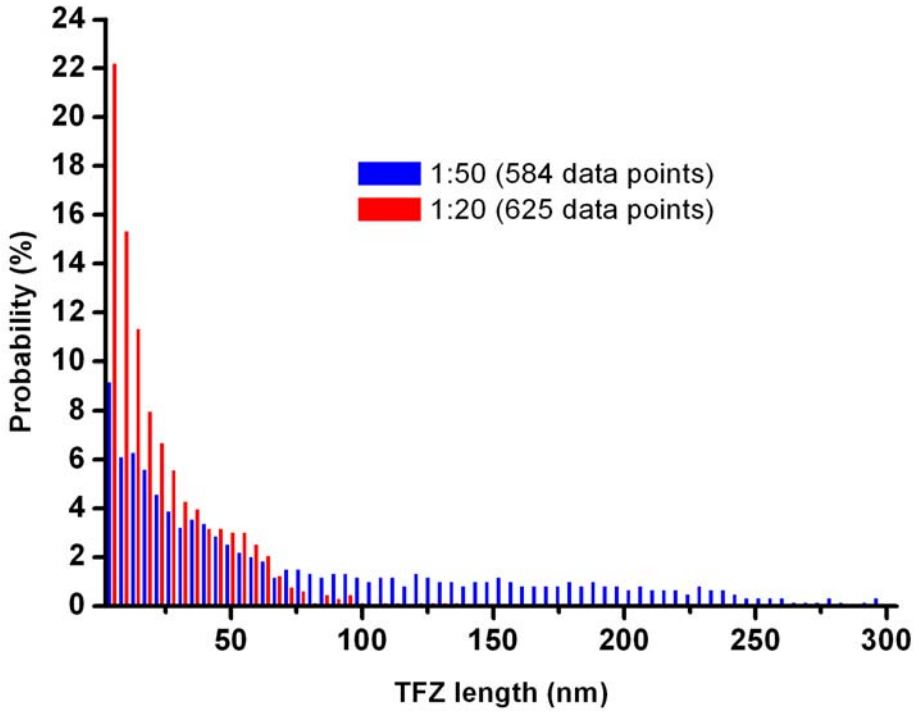

Figure 7. Histograms of TFZ length. The histograms of TFZ length of non-sonicated F-actin depends on the ratio of biotinylated G-actin and unlabeled G-actin. Here the F-actin filaments were polymerized from mixture of biotinylated G-actin and unlabeled G-actin with different ratios (biotinylated : unlabeled = 1: 50, blue; 1: 20, red). They were not sonicated before being applied to the biotin/streptavidin-treated polystyrene surface. Each TFZ length bin is 9 nm.

Using TFZ to select and group data allowed us not only to confirm the binding specificity, but also to control the orientation for G-actin/F-actin interactions: in a lifetime measurement led by a sufficiently long TFZ, the tether force is applied along the axial direction of the stretched segment of actin filament. Therefore the G-actin/F-actin bond is stressed in an orientation relevant to filament formation.

Binding was specific to the actin/actin interaction as its frequency was suppressed by not coating the cantilever tip with G-actin, by using G-buffer as working buffer, or by adding 100 uM latrunculin A to prevent actin/actin interactions (Fig. 8).

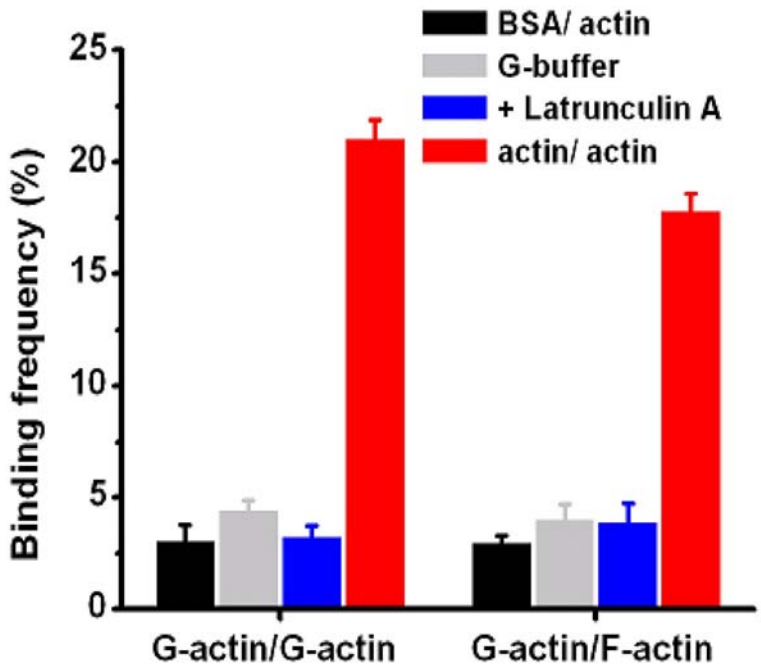

Figure 8. Binding specificity was confirmed for G-actin/G-actin and G-actin/F-actin interactions. The binding frequency of the experimental condition (A, *left and right*) was significantly ($p<0.001$) higher than that of each control condition in which interactions between actins cannot occur (see text descriptions). Data are presented as mean ± s.e.m. of 10-30 binding frequencies for each condition. Each binding frequency was estimated from the number of binding events in 100-200 contacts.

Lifetimes of the serial bonds (in which a G-actin/G-actin or G-actin/F-actin bond was sandwiched between biotin/streptavidin bonds) were specifically terminated by dissociation of the actin/actin bond, not the biotin/streptavidin bond, because the biotin/streptavidin bond alone lasted several hundred-fold longer (Fig. 9). For G-actin/F-actin interactions, the dissociation of the actin/actin bond is most likely to occur at the end, but not the middle of the F-actin, as the force required to rupture the actin filament from the middle is an order of magnitude higher than the force applied in our experiments (Ferrer et al., 2008; Kishino and Yanagida, 1988). Moreover, SMD simulations performed by Dr. Jizhong Lou showed that the actin monomer at the end of F-actin is

always the first subunit to dissociate when the pulling force was applied to the end of the actin filament along its axial direction (See 4.2 Discussion).

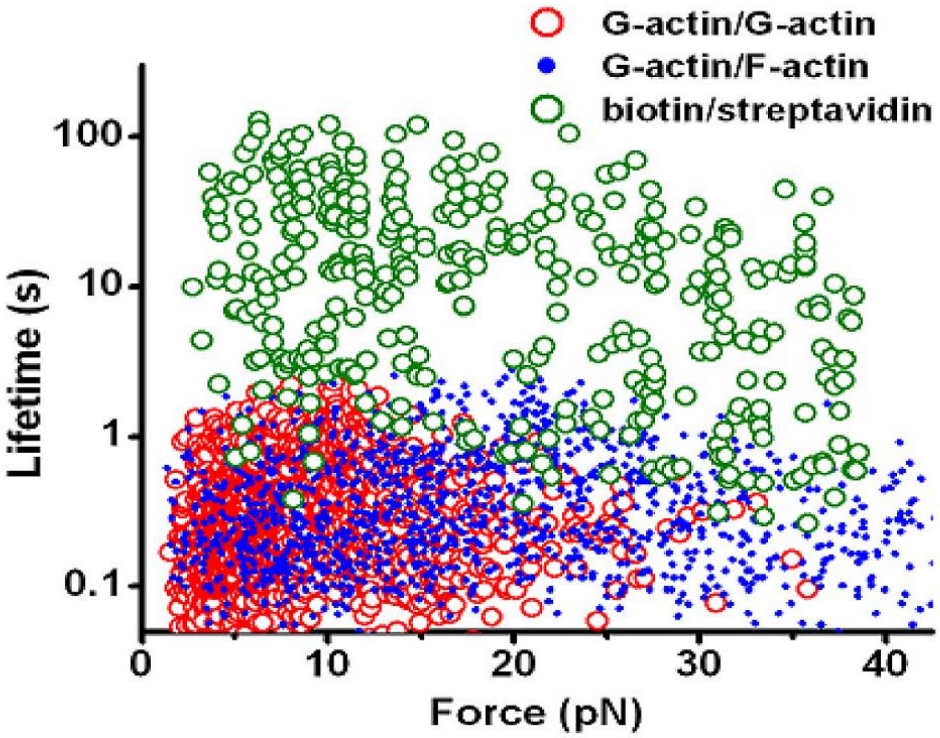

Figure 9. Scatter plots of force-lifetime measurements. The lifetime distribution of the control condition (A, *middle*) allowing biotin/streptavidin interactions only (green) was several hundred-fold longer than that of the experimental condition (A, *left and right*) allowing G-actin/G-actin (red) and G-actin/F-actin (blue) interactions.

3.2 Force regulates dissociation kinetics of actin subunit interactions by catch-slip bonds

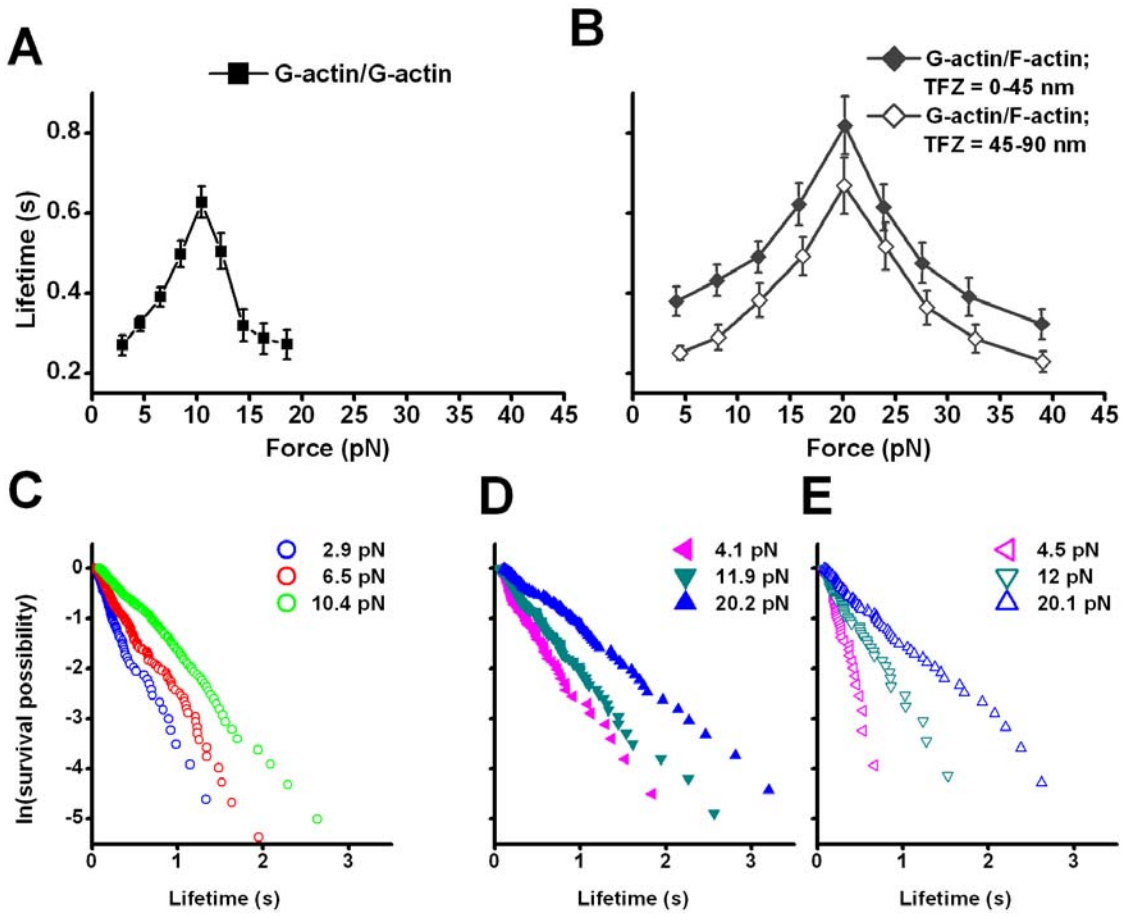

Figure 10. Demonstration of actin catch-slip bonds. (A) Bond lifetimes of the G-actin/G-actin interaction exhibit biphasic force dependence, i.e., catch-slip bonds. (B) Catch-slip bonds for the G-actin/F-actin interactions with TFZ of 0-45 nm (diamond) and 45-90 nm (open diamond). Each point represents the mean ± s.e.m. of > 50 measurements. (C, D, E) Single exponential lifetime distributions exemplified by the linear semi-log plots of survival frequency (i.e., fraction of bonds survived longer than a given time) vs. time for the (C) G-actin/G-actin interaction, (D) G-actin/F-actin interaction with TFZ of 0~45 nm and (E) G-actin/F-actin interaction with TFZ of 45~90 nm, at three representative force bins.

The bond lifetime of G-actin/G-actin interactions exhibited a biphasic "catch-slip" force dependence. It had a "catch bond" region characterized by increasing lifetimes as force increased, with a maximum of 0.63 s at 10 pN, followed by a "slip bond" region within which the lifetimes decreased monotonically as force further increased (Fig. 10A).

Catch-slip bonds of G-actin/F-actin interactions had qualitatively similar but quantitatively different characteristics from those of G-actin/G-actin interactions (Fig. 10B). They had a maximum lifetime of 0.82 s (for data with TFZ = 0-45 nm, roughly equal to 0-15 actin mononer subunits (Holmes et al., 1990)) or 0.67 s (TFZ = 45-90 nm; 15-30 actin monomer subunits) at 20 pN. The bond lifetimes of the group with a TFZ 0-45 nm were universally longer than those of the group with TFZ 45-90 nm, probably because the bindings of the latter group spent a longer time in TFZ and TFZ was not counted into the lifetimes for analysis.

The bond survival probabilities at various force bins for G-actin/G-actin interactions (Fig. 10C) and for G-actin/F-actin interactions grouped with different TFZ (Fig. 10D, 10E) followed single exponential decay, which suggests first-order dissociation kinetics from homogeneous states.

3.3 K113S mutation on yeast actin suppresses actin catch-slip bonds

We tested the bond lifetime-force relationship of G-actin/G-actin interactions using wild type yeast actin in our AFM assay system. The wild type yeast actin preserved the G-actin/G-actin catch-slip bonds similar to those of muscle actin, qualitatively and quantitatively (Fig. 10A and Fig. 11A). The interactions between wild type yeast G-actin and muscle F-actin also exhibited the catch-slip behavior similar to those in pure muscle actin system (Fig. 10 and Fig. 11B).

Mutating the Lys113, which is a positively charged residue, to Ser, which is a hydrophilic non-charged residue, suppressed the catch-slip bonds in both G-actin/G-actin and G-actin/F-actin interactions (Fig. 11A, B).

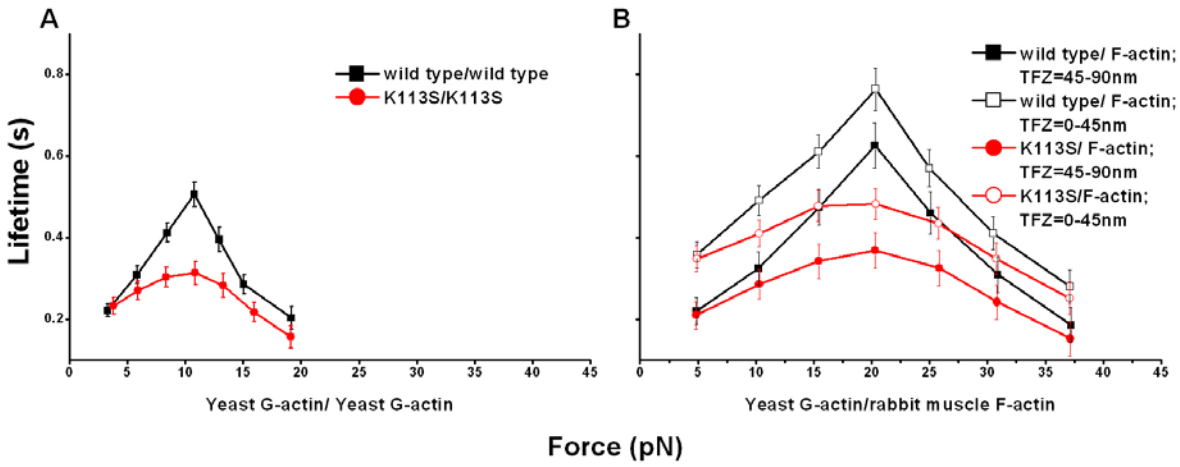

Figure 11. The effect of K113S mutation on actin catch-slip bonds. (A) Wild type yeast actin preserved the G-actin/G-actin catch-slip bonds (black square) while the K113S mutation suppressed the catch-slip bonds (red circle). (B) Catch-slip bonds were preserved in the interaction between wild type yeast G-actin and muscle F-actin (black square). K113S mutation on the yeast G-actin suppressed the G-actin/F-actin catch-slip bonds. actin interactions with TFZ of 0-45 nm (diamond) and 45-90 nm (open diamond). Each point represents the mean ± s.e.m. of > 50 measurements.

3.4 Regulations of actin catch-slip bonds by a RhoA-mDia1 autoinhibition module

We next investigated how the force-dependent actin dissociation kinetics was affected by formin. Addition of different concentrations of the FH2 and DAD domain-containing C-terminal construct of mDia1 (mDia1 C-t) (Fig. 2B), which facilitates actin nucleation (Li and Higgs, 2003, 2005) (Fig. 12), into the working buffer of the G-actin/G-actin assay system converted the catch-slip bonds of G-actin/G-actin interactions to slip bonds in a dose-responsive manner (Fig. 13A). A similar effect was caused by the FH1 and FH2 domain-containing yeast construct Bni1p(FH1FH2)p, which participates in actin nucleation and the assembly of the actin filament barbed end (Fig. 13A) (Kovar and Pollard, 2004; Pruyne et al., 2002). Lifetimes measured in the presence of mDia1 C-t were mediated by specific G-actin/G-actin interactions, as the binding frequency was diminished by conditions preventing these interactions (Fig. 14, *left*).

To investigate the auto-inhibitory effect of the DAD-DID interaction, the DID domain-containing N-terminal construct of mDia1 (mDia1 N-t), which inhibits mDia1 C-t through DAD-DID interactions (Li and Higgs, 2003, 2005) (Fig. 2B, Fig. 12), was added to the mDia1 C-t-containing assay system for G-actin/G-actin interaction. The added mDia1 N-t reversed the mDia1 C-t-induced slip bonds back to catch-slip bonds corresponding to pure G-actin/G-actin interactions (comparing Figs. 10A and 13B).

We further tested the effect of RhoA, which has been shown to relieve the DAD-DID auto-inhibition of mDia1(Li and Higgs, 2003, 2005) (Fig. 2B, Fig. 12). Addition of His-RhoA loaded with GTPγS into our G-actin/G-actin assay system containing mDia1 C-t and mDia1 N-t relieved the auto-inhibitory effect of mDia1 N-t on mDia1 C-t, and thus switched the catch-slip bonds back to slip bonds. The relieving effect of GDP-loaded His-RhoA on mDia1 N-t was less potent than that of His-RhoA loaded with GTPγS (Fig. 13C). His-RhoA and mDia1 N-t together had no effect on G-actin/G-actin interactions, therefore the observed relieving effect of RhoA was specific and depended on rescuing the activity of mDia1 C-t from mDia1 N-t/mDia1 C-t auto-inhibition (Fig. 15).

mDia1 C-t, mDia1 N-t and/or His-RhoA were also tested in the G-actin/F-actin assay system in ways similar to those for G-actin/G-actin interactions. Similar to its effect on G-actin/G-actin interactions (Fig. 13A, 13B, 13C), the RhoA-mediated autoinhibitory module of mDia1 switched the force-dependent lifetimes of G-actin/F-actin interactions between catch-slip bonds and slip bonds (Fig. 13D, 13E, 13F). Lifetimes measured in the

presence of mDia1 C-t were also confirmed to be mediated by specific G-actin/F-actin interactions (Fig. 14, right).

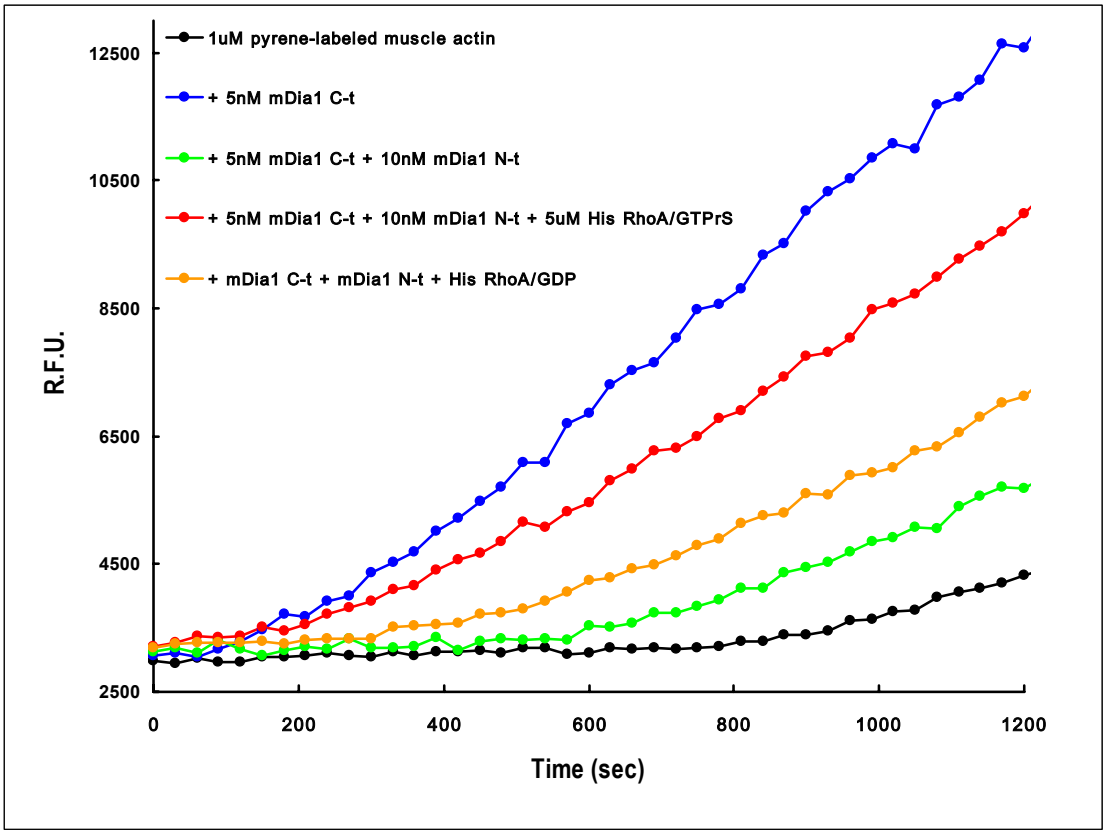

Figure 12. Pyrene-actin polymerization assay. 1 μM pyrene-labeled rabbit skeletal muscle actin was polymerized with mDia1 C-t, mDia N-t, and/or His-RhoA in different nucleotide state, at indicated concentrations. The increase in pyrene fluorescence indicates actin polymerization. The buffer used for the assay is the same as that for AFM experiments. Actin polymerization was enhanced by mDia1 C-t (blue), which was auto-inhibited by mDia1 N-t (green). RhoA relieved the auto-inhibitory of mDia1 N-t on mDia1 C-t but the relieving effect of GDP-loaded His-RhoA on mDia1 N-t was less potent than that of His-RhoA loaded with GTPγS (Red and Orange).

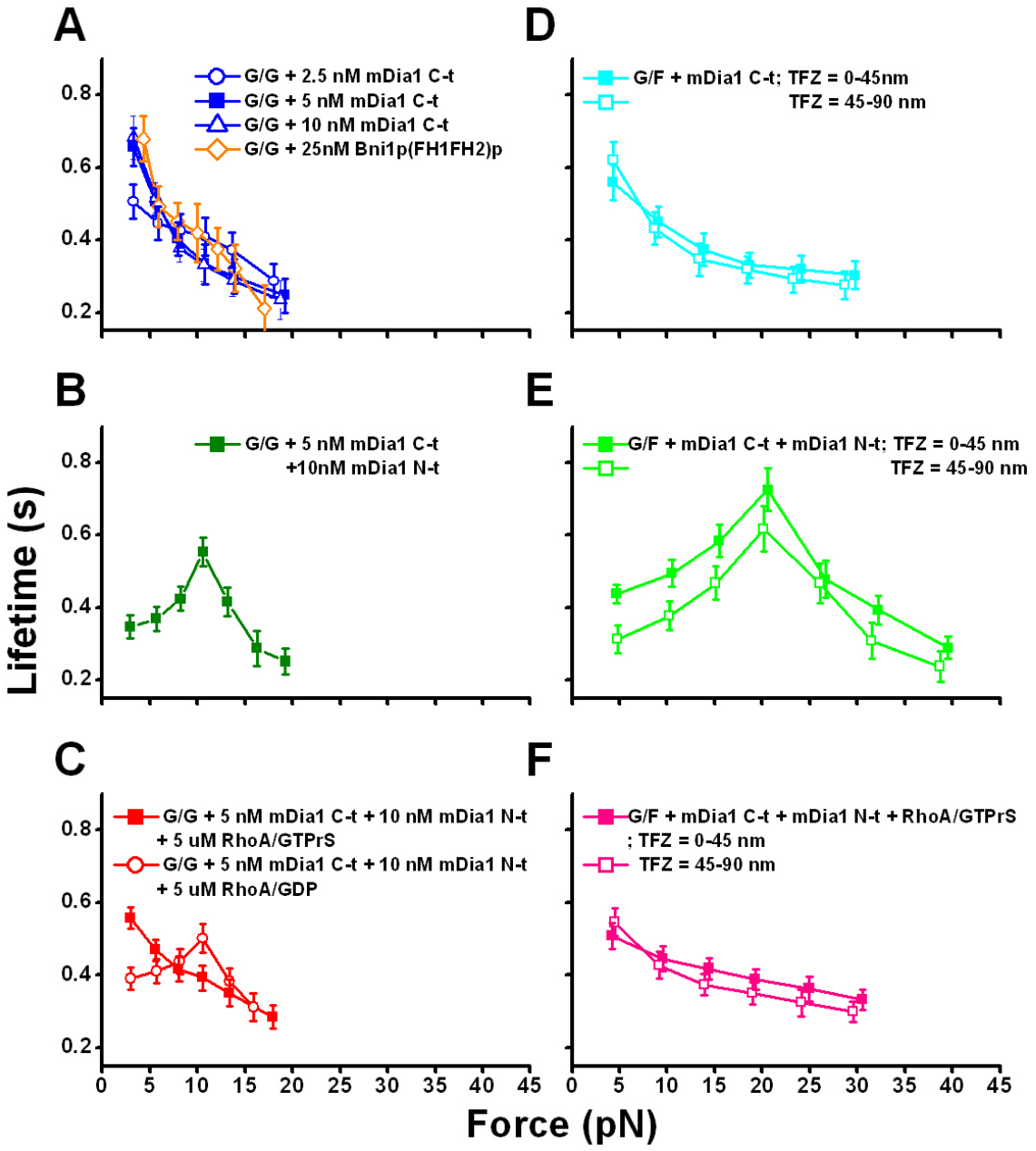

Figure 13. Switching between actin catch-slip bonds and slip bonds by a RhoA-mediated auto-inhibitory module of mDia1. (A) mDia1 C-t (blue symbols) or Bni1p(FH1FH2)p (orange open diamond) converted the G-actin/G-actin catch-slip bonds to slip bonds. (B) mDia1 N-t reversed the mDia1 C-t-induced slip bonds of G-actin/G-actin interactions back to catch-slip bonds. (C) His-RhoA charged with GTPγS (red square) reversed the force-dependent lifetime of G-actin/G-actin interactions back to slip bonds again, by relieving the auto-inhibition of mDia1 N-t on mDia1 C-t. GDP-charged His-RhoA (red open triangle) has less potent relieving effect. (D, E, F) G-actin/F-actin catch-slip bonds were also switched by a RhoA-mDia1 autoinhibitory module. Except for the addition of mDia1 C-t, Bni1p(FH1FH2)p, mDia1 N-t and/or His-RhoA, the experimental parameters in Fig. 5 were the same as those in Fig. 3.

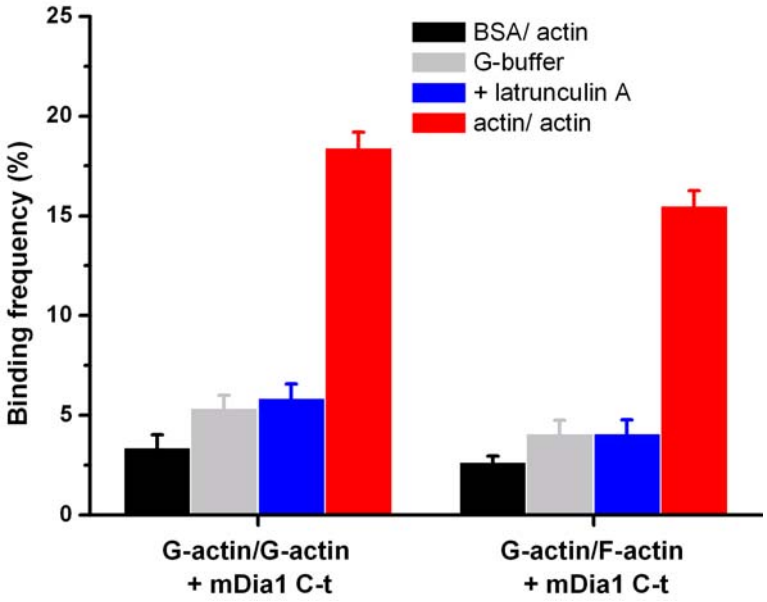

Figure 14. Lifetimes measured in the presence of mDia1 C-t were mediated by specific actin/actin interactions. The binding frequency of G-actin/G-actin (left) and G-actin/F-actin (right) interactions involving mDia1 C-t were significantly ($p<0.001$) higher than that of different control conditions in which interactions between G-actins cannot occur (see Methods Summary). Data are presented as mean ± s.e.m. of 10-30 binding frequencies for each condition. Each binding frequency was estimated from the number of binding events in 100-200 contacts.

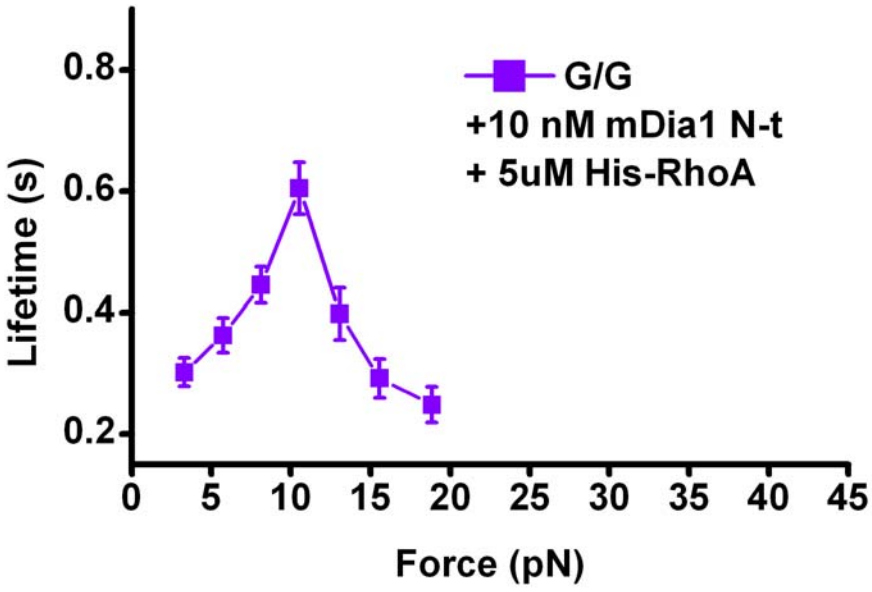

Figure 15. His-RhoA and mDia1 N-t together had no effect on G-actin/G-actin interactions. The observed relieving effect of RhoA was specific and depended on rescuing the activity of mDia1 C-t from mDia1 N-t/mDia1 C-t auto-inhibition.

3.5 CapZ and Tmod3 isolates the specific polar activity in G-actin/F-actin interactions

Considering the polarity of F-actin, it is likely that our bond lifetimes-force measurements of G-actin/F-actin interactions are combinations of barbed-end and pointed-end activities. To isolate the activity of a specific single end from the mixed measurements, we tested the effects of CapZ, which tightly caps the barbed-end of the actin filament, blocks the actin dynamics and competitively inhibits the association of formin to F-actin at the barbed-end (Zigmond et al., 2003). Also we tested the effects of Tmod3, which inhibits the activity at the pointed-end (Babcock and Fowler, 1994; Fischer et al., 2003) (Fig. 16).

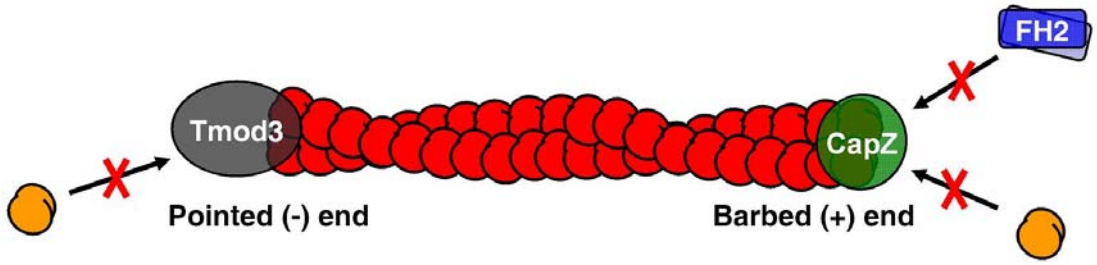

Figure 16. Effects of CapZ and Tmod3 on actin dynamics. CapZ blocks the association of actin monomer and formin onto the barbed end of the actin filament. Tmod3 inhibits the actin dynamics at the pointed end.

Addition of CapZ into the G-actin/F-actin assay system suppressed the binding frequency from 18% to 8%, due to the blockage of interactions at the barbed-end. By capping at the pointed-end, Tmod3 lowered the G-actin/F-actin binding frequency to 13%. Furthermore, adding CapZ and Tmod3 together at the sample time blocks both barbed

and pointed ends, thus the binding frequency of G-actin/F-actin interactions was diminished to that of non-specific background level (3-4%) (Fig. 17).

The binding frequencies with CapZ or Tmod3 were further diminished by conditions that prevent G-actin/F-actin interactions (Fig. 17). This, along with the TFZ (which was not present in control conditions) confirms that the lifetimes measured with CapZ or Tmod3 were specific to G-actin/F-actin interactions.

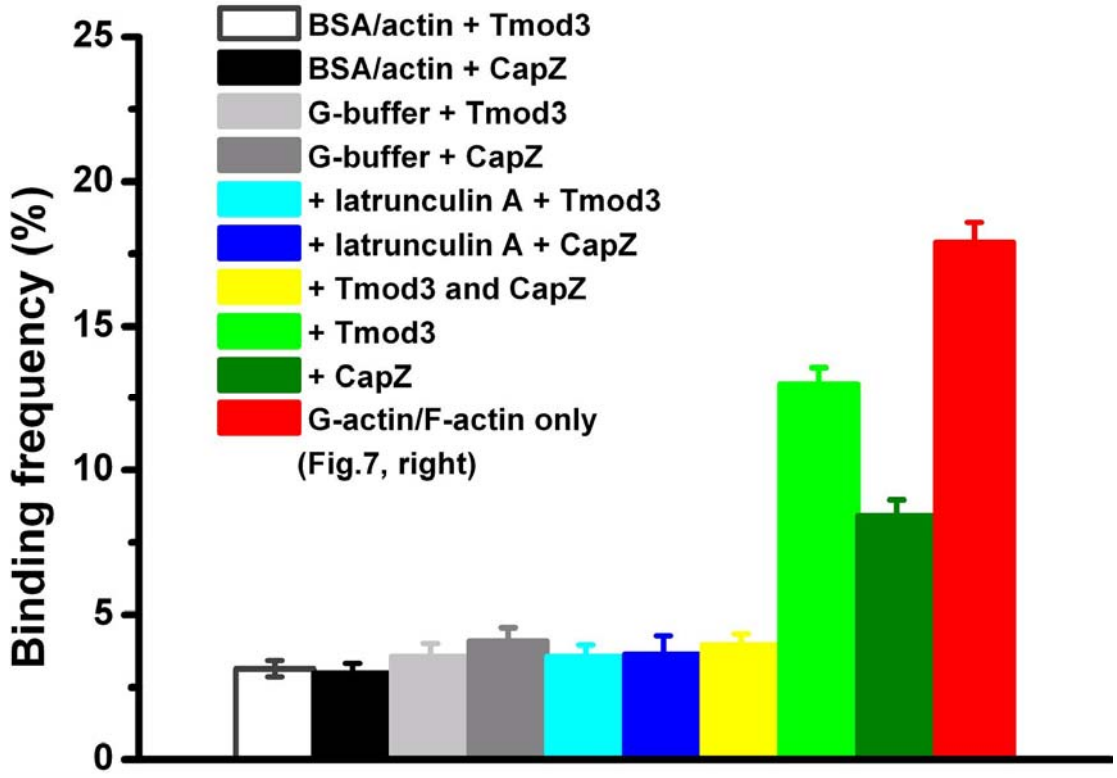

Figure 17. The binding frequency of G-actin/F-actin interactions was suppressed by CapZ and/or Tmod3. It was lowered further in control conditions in which actin/actin interactions can not occur.

The catch-slip bonds of G-actin/F-actin interactions were preserved despite the addition of CapZ or Tmod3 (compare Fig. 18A. 18B, 18C). This suggests that force-

dependent lifetimes of G-actin/F-actin interaction at the pointed-end were qualitatively similar to those at the barbed-end.

Adding mDia1 C-t into the G-actin/F-actin assay system containing CapZ had no effect on G-actin/F-actin interactions (compare Fig. 18D, 18E). In the presence of Tmod3, mDia1 C-t converted the G-actin/F-actin catch-slip bonds to slip bonds with a more significant trend, comparing to that without Tmod3 (compare Fig. 18D, 18F). These results indicate that the catch-slip switching effect of mDia1 C-t specifically occurred at the barbed-end of the actin filament.

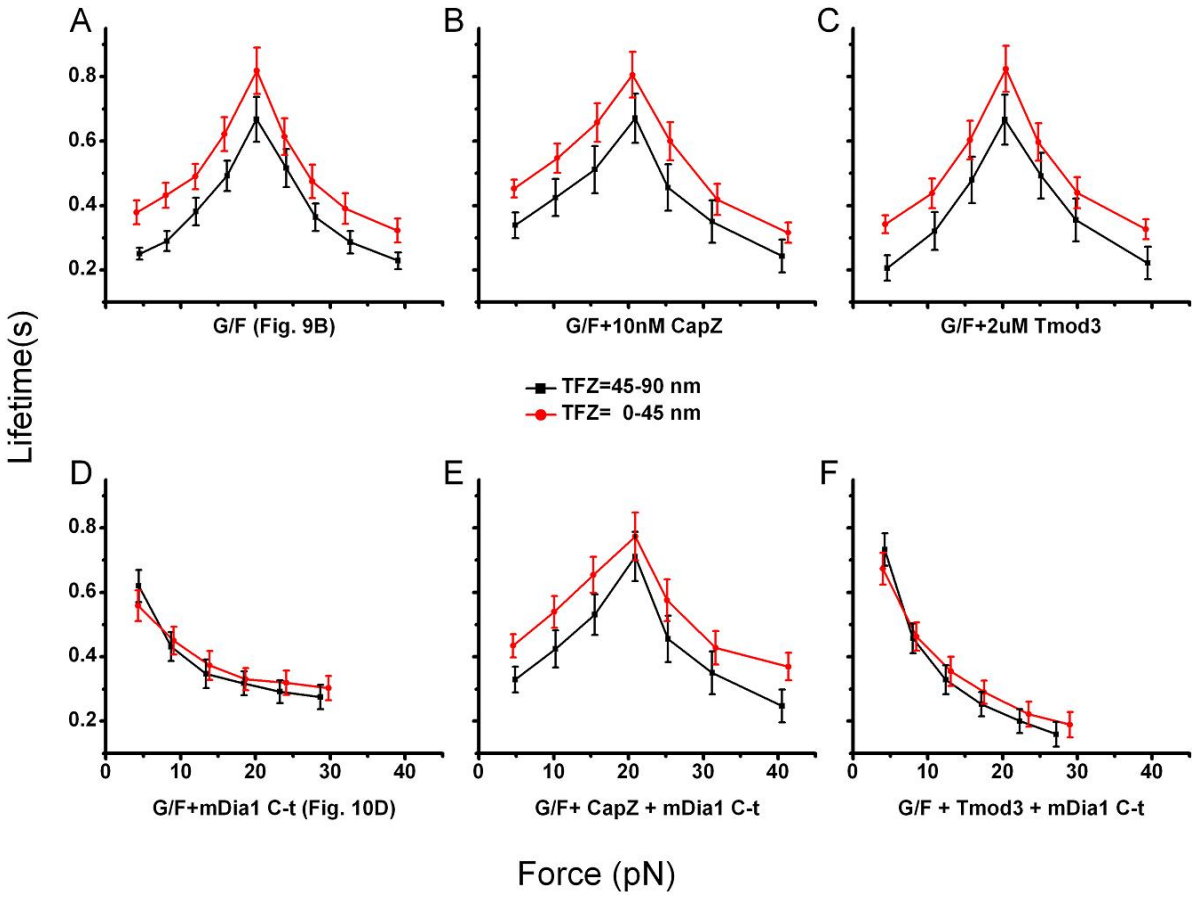

Figure 18. Bond lifetime-force relationship of G-actin/F-actin interactions in the presence of mDia1 C-t, CapZ and/or Tmod3.

CHAPTER 4: Discussion

4.1 Actin dissociation kinetics

Actin filaments in the cytoskeleton are constantly under tensile force and are highly dynamic. The artificial rupture of actin filaments under tension and twist has been studied (Kishino and Yanagida, 1988; Tsuda et al., 1996). Also the effects of compression load on the growing velocity of the actin network have been analyzed (Parekh et al., 2005). However, the effects of tensile force on actin depolymerization have not yet been investigated. Our study on the force-regulated actin subunit interactions represents an *in vitro* model for dissociation of the actin nucleus and the depolymerization of the actin filament ends under tensile force.

Depolymerization of the terminal actin subunit from the filament tip involves dissociation of two G-actin/G-actin bonds (intra-strand; long-pitch and inter-strand; short-pitch) arranged in parallel (Holmes et al., 1990; Howard, 2001). Therefore each component G-actin/G-actin bond at the G-actin/F-actin interface sustains roughly half of the force applied to stretch the actin filament. This can possibly explain our observation showing that the force scale of G-actin/F-actin catch-slip bonds is twice as large as that of G-actin/G-actin catch-slip bonds (compare Fig. 10A, 10B).

Fitting the bond survival probabilities-time curves with the single exponential formula corresponding to first-order dissociation kinetics yielded a dissociation rate constant (k_{off}) of 2.7 s^{-1} or 6.7 s^{-1} for G-actin/F-actin interactions with a TFZ of 0-45 nm

or 45-90 nm, respectively , at the smallest force measured (Fig. 10D, 10E). These values are close to the k_{off} describing the depolymerization at the ends of actin filaments (Pollard, 1986). However, as the first measured off-rate for G-actin/G-actin interactions (Fig. 10C), 3.6 s^{-1} is much smaller than the k_{off} of actin dimers predicted by computer simulations performed under solution-based force-free assumptions (Sept and McCammon, 2001). These assumptions are different from our surface-based system in which both interacting G-actin molecules were immobilized on the AFM probes and dissociated under force. Our surface-based G-actin/G-actin kinetics assay is closer to that seen for G-actin/F-actin interactions, in which the actin molecules are restricted by the adjacent subunits at the filament tips. Other surface-based kinetics studies also obtained kinetic parameters indicating much more stable binding than those measured by solution-based techniques (Cushing et al., 2008)

Quantitatively, at low forces near zero the bond lifetimes of the CapZ-included interactions (pointed-end) were slightly lower than those of the Tmod3-included interactions (compare 18B, 18C). This is consistent with previous studies showing that the dissociation of the actin monomer from the end of the actin filament is faster at the barbed-end than that at the pointed end (Pollard, 1986; Pollard and Borisy, 2003).

4.2 Structural explanation of actin catch-slip bonds provided by SMD simulations

To provide a structural mechanism explaining actin catch-slip bonds, Dr. Jizhong Lou has used SMD simulations (See Appendix I for detailed methods) to study the force-induced actin dimer dissociation and actin filament depolymerization, by

pulling the G-actins within the dimer apart and by pulling the ends of an actin 14-mer filament along its axial direction, respectively (Fig. 19).

For the actin dimer dissociation, simulations were performed with the long-pitch (parallel, intra-strand) and short-pitch (anti-parallel, inter-strand) actin dimers, each of which included G-actins charged with two different nucleotides (ATP or ADP). Pulling caused a relative sliding, enabling the formation of new interactions which tightened the binding between two interacting G-actins (Fig. 19A , 19B). For example, in the long-pitch dimer, salt bridges were formed between Arg39 of the constrained G-actin and Asp286 of the pulled G-actin (Fig. 19A, 19E). In the short-pitch dimer, formation of two salt bridges was observed; one between Glu195 of the constrained G-actin and Lys113 of the pulled G-actin and the other between Arg62 of the constrained G-actin and Glu270 of the pulled G-actin (Fig. 19B, 19F). The new interactions did not occur in control free dynamics simulations without the applied pulling force. These observations were consistent with G-actins charged with two different nucleotide states.

For the actin filament depolymerization, simulations were performed by pulling the terminal actin monomer subunit of an actin 14-mer filament at either the barbed or pointed end while constraining two actin subunits at the other end. In either case, the pulling-induced dissociation occurred at the G-actin/F-actin interface of the pulled end, but not the middle of the filament. This supports the proposal that in AFM experiments for G-actin/F-actin interactions (Fig. 5, *right*) we measured the bond lifetimes corresponding to dissociation of the terminal actin monomer from the end of the filament.

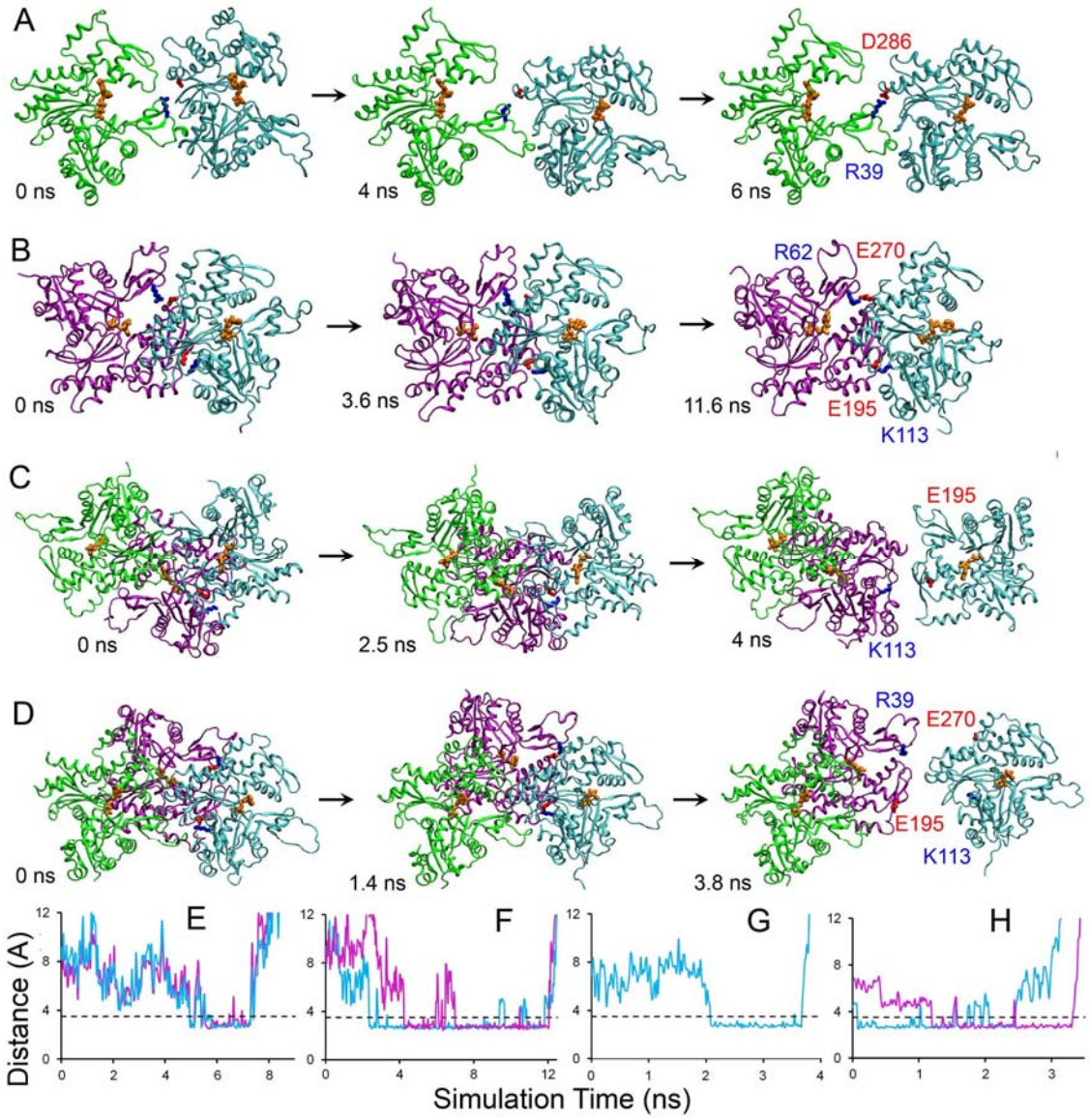

Figure 19. SMD simulated actin dimer dissociation and filament depolymerization under force. (A, B, C, D) Sequential snapshots showing force-induced formation of new interactions within long (A) and short (B) pitch actin dimers, and actin 14-mer filament pulled at the barbed (C) or pointed (D) end. Each panel represents ≥ 3 simulations. For actin dimers, pulling caused a relative sliding between the pulled (cyan) and the constrained (green in A and purple in B) G-actins charged with ATP (green). This enabled the formation of new interactions between acidic (red) and basic (blue) residues that were far apart before pulling, and therefore tightened the binding between G-actins. (C, D) In actin 14-mer filament (only 3 subunits were shown) pulled at either barbed (C) or pointed (D) end, only the pulled terminal subunit (cyan) dissociated from the rest of actin filament. Pulling-induced relative sliding and formation of new interactions were also observed in actin filament depolymerization. (E, F, G, H) Time courses of the distances between the interacting atoms of the representative residues involved in the pulling-induced new interactions shown in (A, B, C, D), respectively (see text for details). Inter-atomic distances shorter than 3.5 Å (horizontal dashed line in E-H) indicate the formation of noncovalent interactions between the interacting atoms. Provided by Dr. Jizhong Lou (Institute of Biophysics, Chinese Academy of Sciences, Beijing, China)

Pulling-induced new interactions were also observed for actin filament depolymerization. For example, when pulling was applied to the barbed end, a salt bridge between Glu195 of the pulled actin subunit and the Lys113 of the neighboring inter-strand subunit in the constrained filament was observed (Fig. 19C, 19G). When pulling was applied at the pointed end, formation of two salt bridges was observed; one between Lys113 of the pulled actin subunit and Glu195 of the neighboring inter-strand actin subunit, and another between Glu270 of the pulled actin subunit and Arg39 of the neighboring inter-strand actin subunit (Fig. 19D, 19H).

The sliding-rebinding model, based on previous SMD simulations of selectin/ligand (Lou and Zhu, 2007) and GPIbα/VWF-A1(Yago et al., 2008) dissociations with results similar to our observations, has been proposed to explain the catch bonds of these systems. This model might also be applicable for the G-actin/G-actin or G-actin/F-actin interactions: at low forces, the actin/actin bond can dissociate directly without forming any new interaction. As force increases, the force-induced sliding along the interface between the interacting actins allows the formation of new strong interactions, which prolongs the overall bond lifetime and gives rise to catch bonds.

The pulling-induced formation of salt bridge between Lys113, a positive-charged amino acid residue, of one actin monomer and Glu195, a negative-charged amino acid residue, of the neighboring inter-strand actin monomer was observed in the simulations for the short-pitch actin dimer dissociation and for the actin filament depolymerization at both barbed and pointed ends, suggesting the importance of this pair of residues.

Using the yeast actin, which has the catch-slip behaviors similar to those of muscle actin (Fig. 11), as a model, we have shown that the actin catch-slip bonds was suppressed by the K113S mutation (compare Fig. 10 and Fig. 11). K113S has a hydrophilic non-charged residue Ser replacing Lys113, therefore is not able to form a salt bridge with Glu195 on the other actin. Besides, it has similar kinetic properties as wild type yeast actin (Fig. 20) (unpublished data from Dr. Peter A. Rubenstein's lab) at force-free condition. These altogether supports the hypothesis that the force-induced formation of Lys113:Glu195 salt bridge is the one of the structural causes of actin catch bond.

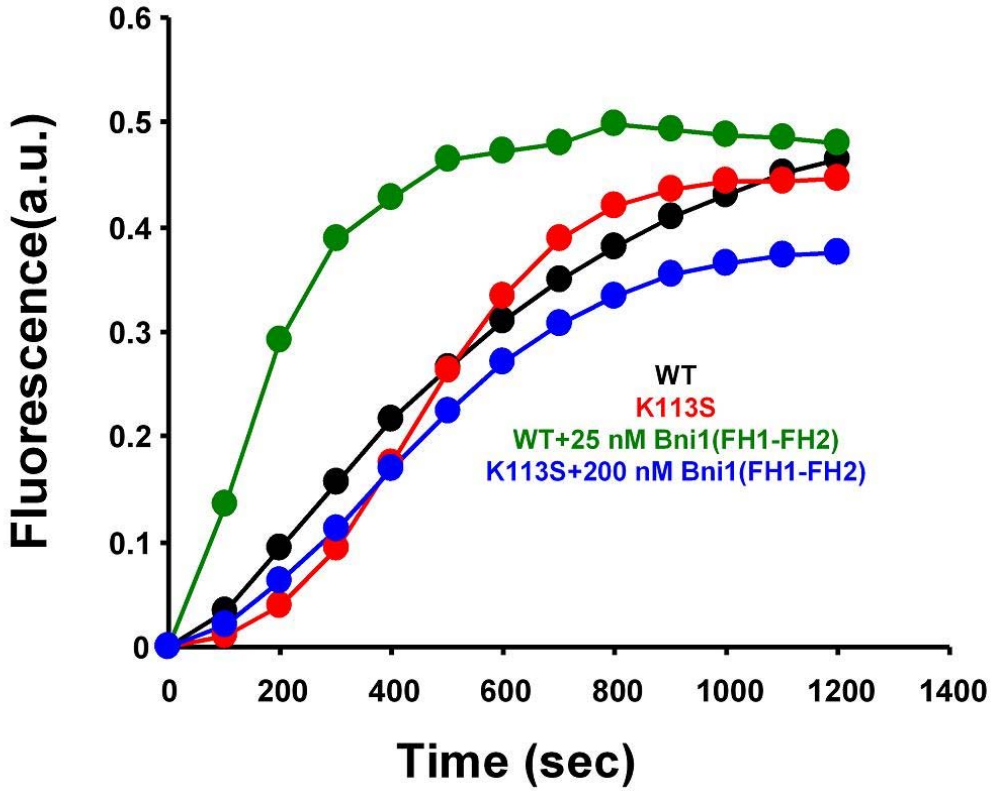

Figure 20. Pyrene-actin polymerization assay of yeast actin. 2 µM wild-type yeast actin(WT) or K113S yeast actin mutant containing 5% pyrene-labeled WT actin was polymerized with or with 25 nM (for WT actin) or 200 nM (for mutant actin) Bni1(FH1-FH2). The increase in pyrene-fluorescence indicates actin polymerization. Provided by Peter A. Rubenstein's group (University of Iowa).

4.3 The switching effect of the formin FH2 domain on actin catch-slip bonds

In the presence of FH2 domain-containing mDia1 C-t or Bni1p(FH1FH2)p, the bond lifetimes of actin subunit interactions were prolonged at low forces (and extrapolation to zero force) (compare Fig. 10A and 13A; 10B and 13D). This is consistent with the previously reported force-free estimations that the FH2 domain stabilizes the actin dimer and the barbed-end of the actin filament (Paul and Pollard, 2008, 2009; Pring et al., 2003; Zigmond, 2004).

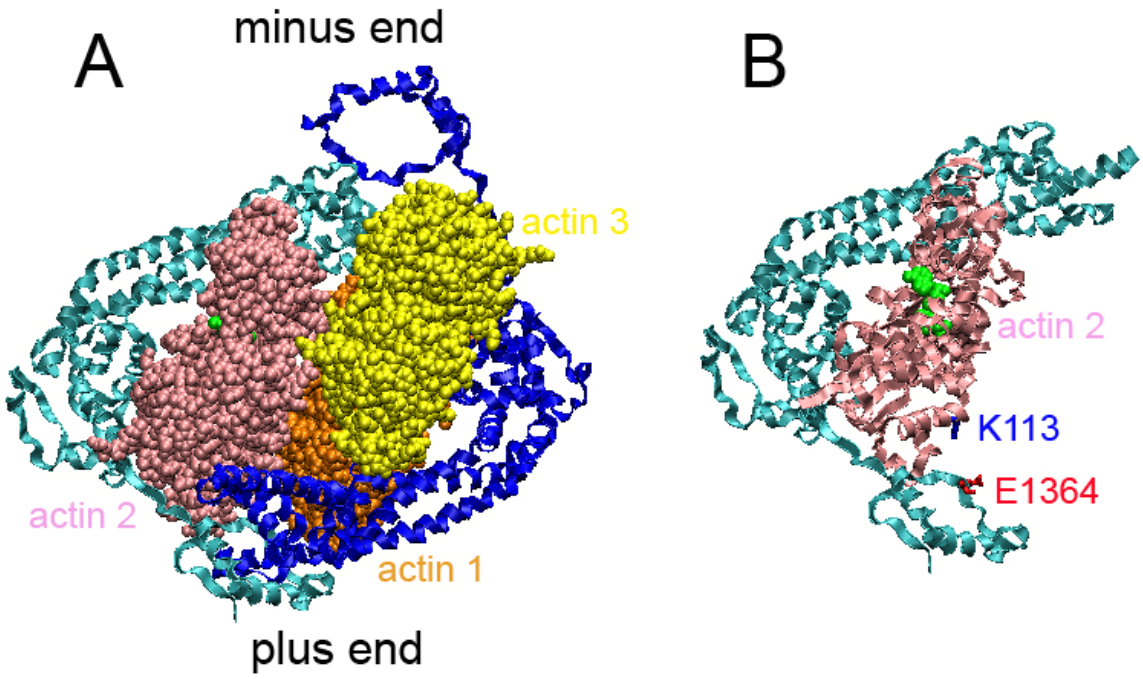

Figure 21. Structure of the FH2-actin complex. (A) Stereo view of the structure of dimeric Bni-FH2 ring (blue and cyan) binding to actin subunits (orange and pink and yellow). (B) Detailed view of the contact area between the cyan FH2 domain and the pink actin 2 demonstrated in (A). The key residues constituting the FH2-actin contact area are listed. Adapted and modified from (Otomo et al., 2005)

The crystal structure of FH2 domain (Xu et al., 2004) and actin-FH2 complex (Otomo et al., 2005) suggests that two FH2 domains form a dimeric ring binding to short-pitch actin dimer and thus two inter-stand actin subunits (short pitch-oriented) at the

barbed-end of the actin filament (Fig. 21A). This ring-like FH2-actin complex structure can possibly explain that FH2 domain stablizes the actin dimer and the F-actin barbed end in force-free environment.

In the crystal structure of actin-FH2 complex the Lys113 residue of an actin subunit is closely located to the Glu1364 residue of a FH2 domain (Fig. 21B). It was shown in an unpublished force-free actin polymerization study (Dr. Peter A. Rubenstein's lab, University of Iowa) that mutating the Lys113 residue to Ser113 (K113S) in yeast actin eliminated the effect of FH2 on actin polymerization (Fig. 20). These results suggest the importance of actin Lys113 in formin-actin interactions.

Besides, this actin Lys113 was also suggested to be a key residue contributing the force-induced new interactions (Lys113: Glu195), a possible structural explanation for actin catch bonds (see 3.3, Fig. 11, K113S mutagenesis study and 4.1 Fig. 19, SMD simulations by Dr. Jizhong Lou). Therefore the mechanistic explanation for the results that FH2-containing formin constructs eliminated the catch-bond phenomenon of actin subunit interactions could be the inhibition of the force-induced new interaction between actin Lys113 and Glu185, by FH2 Glu1364 residue, which occupies the binding site of actin Lys113.

Further more, the spring-like linker structure connecting the dimeric FH2 ring in the functional actin-FH2 complex (Otomo et al., 2005; Paul and Pollard, 2008; Xu et al., 2004) suggests that force might lower the energy barrier caused by the spring-like hindrance thus facilitate the escape of the actin monomer from the bound complex with

formin. This is consistent with the FH2-containing mDia1 C-t-induced slip bonds we observed.

4.4 The physiological significance of switchable actin catch-slip bonds

The force range of the actin catch-slip bonds we observed (20 pN for G-actin/F-actin interactions, the force corresponding to maximal bond lifetime) is relevant to the physiological force-bearing function of actin filaments, as it matches the estimated tensile force magnitudes sustained by a single actin filament *in vivo*. For example, it has been shown that the yield strength of a single actin filament is 3-30 pN (Adami et al., 2002; Grazi et al., 2004); the isometric force that a single myosin molecule exerts on a single actin filament is 3-9 pN (Finer et al., 1994; Takagi et al., 2006); and the stretching force that activates talin, a protein that transmits the force from an integrin molecule to an actin filament by sequentially binding to both of them, is 12 pN (del Rio et al., 2009). The force-prolonged bond lifetimes, i.e. catch bonds, at a force regime physiologically sustained by a single actin filament can possibly explain *in vivo* tension-induced actin polymerization and cytoskeleton stabilization (Gunst and Zhang, 2008; Hirata et al., 2008; Kolega, 1986).

The biological relevance of the actin catch-slip bonds is also supported by their regulation by RhoA and mDia1 (Fig. 13). In G-actin/F-actin interactions, the regulated switch from catch-slip bonds to slip bonds shifts the force that corresponds to the maximal bond lifetime from 20pN to nearly zero (Fig. 10B and Fig. 13D, 13E, 13F). In the cell subjected to directional forces, this switchable force dependence of actin bond lifetime can result in its anisotropic variation, which causes the anisotropic stability of the

actin network. Therefore it may lead to the directional alignment of the actin cytoskeleton in cells sustaining anisotropic forces, depending on the activity of RhoA and mDia1. For example, Kaunas *et al.* have observed that the cell and its actin stress fibers align perpendicular to the cyclic uniaxial stretch direction when RhoA and mDia1 are involved, and the alignment is parallel to the stretch direction if RhoA or mDia1 is compromised (Kaunas et al., 2005) (Fig.3). These observations imply that with mDia1 and RhoA, the actin cytoskeleton is most stable in the minimal force direction (perpendicular to stretch); and the direction with the most stability will be shifted to that with the maximal force (parallel to stretch) if mDia1 or RhoA is suppressed. This might be explained by our findings that the actin dissociation kinetics depend on force in a catch/slip switching fashion controlled by the RhoA/mDia1 pathway.

Since theoretically predicted (Dembo et al., 1988) and first demonstrated (Marshall et al., 2003), catch-slip bonds have been observed in several distinct molecular interactions that bear loads as part of their *in vivo* functions(Guo and Guilford, 2006; Kong et al., 2009; Yago et al., 2008; Yakovenko et al., 2008). Our observations on actin support the hypothesis that catch-slip bonds represent an important functional mechanism for the force-regulation of bio-molecular interactions.

4.5 The potential pathological implication of actin catch-slip bonds

Nemaline myopathy (NM), or rod myopathy is a congenital neuromuscular disorder causing skeletal muscle weakness at proximal muscle groups, including respiratory, bulbar and trunk muscles. NM patients usually suffer from delayed motor development and babies with NM are frequently hypotonic. The patients born with NM

usually gain strength as they grow but the symptoms caused by muscle weakness may progress with time. NM has been divided into six clinical subtypes: severe, intermediate, typical and mild (all congenital); adult-onset, and other forms (Laing et al., 2009; Vinay Kumar et al., 2010).

The pathological findings of NM are primarily on skeletal muscle tissue. The biopsy of the muscle tissue from NM patients shows rod-shaped intra-cytoplasmic inclusions called Nemaline bodies. Though they are the diagnostic criterion of NM, they may be the consequence, but not the cause, of the disease (Vinay Kumar et al., 2010).

The congenital NM shows genetic heterogeneity. It can be caused by mutations in the alpha-actin-1 gene (ACTA1; OMIM#102610) on chromosome 1q42, the tropomyosin-3 gene (TPM3; OMIM#191030) on chromosome 1q22, the nebulin gene (NEB; OMIM#161650) on chromosome 2q22, the beta-tropomyosin gene (TPM2; OMIM#190990) on chromosome 9p13, the troponin T1 gene (TNNT1; OMIM#191041) on chromosome 19q13, and the cofilin-2 gene (CFL2; OMIM#601443). These different genes each encode a component of skeletal muscle sarcomeric thin filaments (Laing et al., 2009; Sanoudou and Beggs, 2001).

Among the genetic causes for NM, ACTA1 mutations are the second most common cause of cause of NM (mutations in NEB are the most common cause), and are the dominant cause in the severe subtype with early death (Laing et al., 2009).

In the SMD simulations performed by Dr. Jizhong Lou (sec. 4.2, Fig. 19), force-induced formation of new salt bridges between the surface residues of the interacting actins were proposed to be a structural mechanism of actin catch-slip bonds.

Our experimental data showing that the actin K113S mutation suppressed the actin catch-slip bonds further supports this idea.

Among the residues contributing the force-induced new interactions in the SMD simulations, 4 out of 6 of them have been reported to be involved in the ACTA1 mutations causing NM: R39X, K113E, E270Q, D286G (Laing et al., 2009). Remarkably, ACTA1 D286G transgenic mouse has been characterized as a model for NM (Feng et al., 2009). These results support the physiological importance of actin catch-slip bonds in maintaining normal muscle phenotype and the potential pathological implication of the actin catch-slip bonds in NM pathogenesis.

CHAPTER 5: CONCLUSION

5.1 Summary

In this study the bond lifetime-tensile force relationships of G-actin/G-actin and G-actin/F-actin interactions were measured at the single-bond level by AFM force-clamp experiments. We demonstrated that the dissociation kinetics of G-actin/G-actin and G-actin/F-actin interactions are regulated by force though catch-slip bonds (Fig. 10), which can be explained by force-induced formation of new interactions between adjacent interacting actin subunits – a structural mechanism suggested by SMD simulations (Fig. 19). This structural explanation was supported by the yeast actin mutagenesis study showing that the actin K113S mutation suppressed the actin catch-slip phenotype (Fig. 11). We also showed that the actin catch-slip bonds can be switched to a slip-only phenotype by formin, which is regulated by a RhoA-mediated DAD-DID auto-inhibitory module (Fig. 13).

As the first to investigate the force dependence of actin dynamics at the single-bond level, we provide a molecular-level example for how actin dynamics are regulated by force and how this biophysical regulation is further modulated biochemically. By demonstrating the interplay between actin kinetics, force, RhoA and formin, our study suggests that the RhoA-mediated DAD-DID auto-inhibitory module of mDia1 functions as a "molecular switch" (Hall and Nobes, 2000) controlling the force dependency of actin

dynamics. It thus offers a possible physiological mechanism integrating force and biochemical signaling to control actin reorganization in cells. (Fig. 22 for summary)

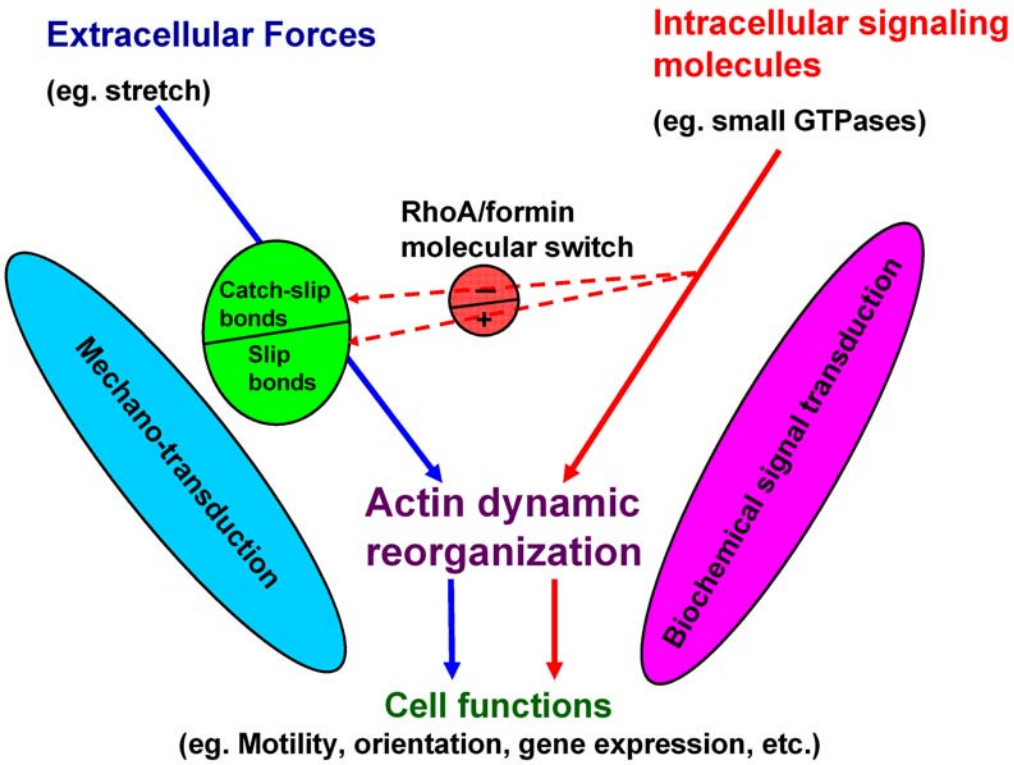

Figure 22. Schematic summary of major concepts. Actin cytoskeleton dynamics which control molecular-level cell functions are regulated by extracellular forces, as these dynamics are crucial to mechanotransduction (blue arrows). They are also regulated by intracellular GTPases, contributing an important framework for biochemical signal transduction (red arrows). Our study demonstrates that force regulates actin dynamics by a catch-slip mechanism (green circle); this biophysical regulation is modulated by biochemical signaling though RhoA and formin (red dashed arrows). The RhoA-formin module can serve as a molecular switch shifting the force dependence of actin dynamics between catch-slip bonds (with inactivated RhoA or formin/-) and slip bonds (with activated RhoA and formin/+) (red circle, dashed arrows and green circle). It illustrates a direct crosstalk between mechanotransduction and signal transduction pathways.

5.2 Future works

5.2.1 Experimental confirmation of the structural mechanism of actin catch-slip bonds

In 4.2 a structural mechanism explanation the actin catch-slip bonds was mentioned, based on the SMD simulations studying the force-induced actin dimer

dissociation and actin filament depolymerization. It was suggested that the pulling force induces the formation of strong ionic bridges between interacting actin subunits, including the salt bridge form between Lys113 and Glu195. The force-induced new interaction caused by the salt bridge of Lys113:Glu195 occurred in the dissociation of short-pitch actin dimer, and both the barbed-end and the pointed end of the actin filament, suggesting the importance of this pair of residues. This hypothesis was supported by the experiment showing that the K113S mutation suppressed the actin catch-slip bonds (Fig. 11). To further confirm this argument, the mutation of yeast actin Glu195, such as E195S, should be tested in our AFM assay system, to see if it can suppress the actin catch-slip bonds as K113S mutant did.

5.2.2 Confirmation of the functional significance of actin catch-slip bonds *in-vivo*

In 4.4 we proposed that the switchable actin catch-slip bonds modulated by a RhoA-formin module can cause the anisotropic stability of actin network subjected to directional stress, thus be a possible mechanism controlling the force-induced intracellular actin stress fiber alignment. Previous *in vivo* study by *Kaunas* et al. showed that the cell and its actin stress fibers align perpendicular to the cyclic uniaxial stretch direction when RhoA and mDia1 are involved, and the alignment is parallel to the stretch direction if RhoA or mDia1 is compromised (Kaunas et al., 2005). These observations are in line with the hypothesis we proposed.

To further test the hypothesis that the actin catch-slip bonds control the force-induced alignment of the cell and its actin stress fibers, other factors able to perturb the actin catch-slip bonds have to be introduced into the cell applied with force.

If the yeast actin mutant E195S mentioned can be verified to eliminate the actin catch-slip bonds as K113S did, each of K113S or E195S mutant can be introduced into the living cell to see if the alignment of the cell and its stress fibers in response to periodic uni-directional stretch can be modulated by the mutants. A plausible way to introduce the actin mutants into cells is microinjection of the fluorescence-labeled purified actin mutants into cultured cells, such as the system described previously (Hayakawa et al., 2001).

5.2.3 Study of the implication of actin catch-slip bonds in NM pathogenesis

In 4.5 we mentioned the potential implication of the actin catch-slip bonds in the NM pathology, based on the correlation of the SMD-simulated structural mechanism (Fig. 19) and the reported ACTA1 mutations causing NM (Laing et al., 2009).

The animal model of NM has been developed, using the D286G transgenic mouse (Feng et al., 2009). In the SMD simulation, the D286: R39 salt bridge induced by pulling force was observed in long-pitch actin dimer, therefore was suspected as a possible structural mechanism for G-actin/G-actin catch bonds. To test this hypothesis, we can test the purified D286G actin mutant obtained from the transgenic mouse in our AFM bond lifetimes- force assay system, to see if the D286G mutation on actin can change the catch-slip phenotype of actin. If so, we can also apply the unidirectional periodic stretch on mouse muscle cells expressing D286G actin mutant, to test the hypothesis that the actin catch-slip bonds control the force-induced alignment of the cell and its actin stress fibers.

In the long term perspective, we can verify the effects of the residues involving the structural mechanism of actin catch-slip bonds (according to the SMD simulation), using the combination of the yeast actin mutagenesis system and our AFM assay system. The next goal can be developing the transgenic mouse model expressing the actin mutants affecting actin catch-slip phenotype. Upon accomplishing these goals, we can observe the phenotype caused by perturbing the actin catch-slip bonds, at cellular level, tissue level, organ level and body system level, in the transgenic mice. By these perspective achievements we can possibly define the relationship between actin catch-slip bond and NM, therefore leading to possible treatments of the disease.

APPENDIX
SMD simulation protocol (provided by Dr. Jizhong Lou)

MD simulations were performed using the NAMD program(Phillips et al., 2005) under CHARMM22 all-atom force field with CMAP correction for protein(MacKerell et al., 1998). The coordinates for long- and short-pitch dimers and actin 14-mer filaments were obtained by taking the corresponding portion from a recent F-actin model (PDB code 2ZWH)(Oda et al., 2009). In the dimer structures, ADPs were replaced with ATPs by aligning each monomer with the ATP actin structures (Graceffa and Dominguez, 2003; Holmes et al., 1990) (PDB code 1ATN and 1NWK). Crystallized water molecules that are important to ATP binding and metal ion coordination in 1NWK were kept in our ATP-actin dimer models. Similarly, crystallized water molecules that are important to ADP binding and metal ion coordination in an ADP-actin structure (PDB code 1J6Z)(Otterbein et al., 2001) were included in our actin filament and ADP-actin dimer models. The modeled long- and short-pitch actin dimmers and actin filaments were soaked in water boxes of 512 × 128 × 128 $Å^3$, 180 × 100 × 90 $Å^3$ and 144 × 100 × 90 $Å^3$ with 802,880, 153,836 and 122,132 atoms, respectively, including Ca^{2+} and Cl^- ions to neutralize the environment. The systems were sequentially subjected to 10,000 steps energy minimization with heavy atoms fixed, 10,000 steps with protein heavy atoms fixed, 10,000 steps with only protein C_α atoms fixed, and 10,000 steps with all atoms free. A 12-Å cutoff was used for van der Waals interactions and Particle Mesh Ewald summation was used to calculate the electrostatic interactions in all simulations. The energy-minimized systems were equilibrated for 4 ns with temperature controlled at 310

K using Langevin dynamics and pressure controlled at 1 atm by the Langevin piston method. The equilibrated structures were taken as the starting point for additional 6ns (for actin filament) or 26 ns (for actin dimmers) free dynamics simulations. Steered molecular dynamics (SMD) simulations were performed using different starting conformations resulting from free dynamics simulations. In each SMD simulation for actin dimer systems, the C_α atom of a surface Lys residue from one G-actin was harmonically constrained and the C_α atom of a surface Lys residue from another G-actin was pulled at a constant speed of 0.5 nm/ns with a spring constant 70 pN/nm. The pulling forces were applied via Lys because biotin was attached to this residue in the biotinylated G-actin used in our AFM experiment. Different combinations of constrained and pulled atoms were simulated. Parallel simulations for ADP-bound actin dimers were also performed. For the SMD simulations of the actin filament, the actin subunit at the barbed or pointed end was pulled at a constant speed of 1 nm/ns with a spring constant of 350pN/nm while the two subunits at another end were constrained. Structures in Fig. 4 and the supplemental videos were generated by Visual Molecular Dynamics software (Humphrey et al., 1996).

REFERENCES

Adami, R., Cintio, O., Trombetta, G., Choquet, D., and Grazi, E. (2002). Effects of chemical modification, tropomyosin, and myosin subfragment 1 on the yield strength and critical concentration of F-actin. Biochemistry *41*, 5907-5912.

Alberts, B., Johnson, A., Lewis, J., Raff, M., Roberts, K., and Walter, P. (2002). Molecular biology of the cell, 4th edn (Garland Science).

Babcock, G.G., and Fowler, V.M. (1994). Isoform-specific interaction of tropomodulin with skeletal muscle and erythrocyte tropomyosins. J Biol Chem *269*, 27510-27518.

Chien, S. (2007). Mechanotransduction and endothelial cell homeostasis: the wisdom of the cell. Am J Physiol Heart Circ Physiol *292*, H1209-1224.

Cushing, P.R., Fellows, A., Villone, D., Boisguerin, P., and Madden, D.R. (2008). The relative binding affinities of PDZ partners for CFTR: a biochemical basis for efficient endocytic recycling. Biochemistry *47*, 10084-10098.

del Alamo, J.C., Norwich, G.N., Li, Y.S., Lasheras, J.C., and Chien, S. (2008). Anisotropic rheology and directional mechanotransduction in vascular endothelial cells. Proc Natl Acad Sci U S A *105*, 15411-15416.

del Rio, A., Perez-Jimenez, R., Liu, R., Roca-Cusachs, P., Fernandez, J.M., and Sheetz, M.P. (2009). Stretching single talin rod molecules activates vinculin binding. Science *323*, 638-641.

Dembo, M., Torney, D.C., Saxman, K., and Hammer, D. (1988). The reaction-limited kinetics of membrane-to-surface adhesion and detachment. Proc R Soc Lond B Biol Sci *234*, 55-83.

Etienne-Manneville, S., and Hall, A. (2002). Rho GTPases in cell biology. Nature *420*, 629-635.

Feng, J.J., Ushakov, D.S., Ferenczi, M.A., Laing, N.G., Nowak, K.J., and Marston, S.B. (2009). Direct visualisation and kinetic analysis of normal and nemaline myopathy actin polymerisation using total internal reflection microscopy. J Muscle Res Cell Motil *30*, 85-92.

Ferrer, J.M., Lee, H., Chen, J., Pelz, B., Nakamura, F., Kamm, R.D., and Lang, M.J. (2008). Measuring molecular rupture forces between single actin filaments and actin-binding proteins. Proc Natl Acad Sci U S A *105*, 9221-9226.

Finer, J.T., Simmons, R.M., and Spudich, J.A. (1994). Single myosin molecule mechanics: piconewton forces and nanometre steps. Nature *368*, 113-119.

Fischer, R.S., Fritz-Six, K.L., and Fowler, V.M. (2003). Pointed-end capping by tropomodulin3 negatively regulates endothelial cell motility. J Cell Biol *161*, 371-380.

Fletcher, D.A., and Mullins, R.D. (2010). Cell mechanics and the cytoskeleton. Nature *463*, 485-492.

Grazi, E., Cintio, O., and Trombetta, G. (2004). On the mechanics of the actin filament: the linear relationship between stiffness and yield strength allows estimation of the yield strength of thin filament in vivo. J Muscle Res Cell Motil *25*, 103-105.

Gunst, S.J., and Zhang, W. (2008). Actin cytoskeletal dynamics in smooth muscle: a new paradigm for the regulation of smooth muscle contraction. Am J Physiol Cell Physiol *295*, C576-587.

Guo, B., and Guilford, W.H. (2006). Mechanics of actomyosin bonds in different nucleotide states are tuned to muscle contraction. Proc Natl Acad Sci U S A *103*, 9844-9849.

Hall, A. (1998). Rho GTPases and the actin cytoskeleton. Science *279*, 509-514.

Hall, A., and Nobes, C.D. (2000). Rho GTPases: molecular switches that control the organization and dynamics of the actin cytoskeleton. Philos Trans R Soc Lond B Biol Sci *355*, 965-970.

Hayakawa, K., Sato, N., and Obinata, T. (2001). Dynamic reorientation of cultured cells and stress fibers under mechanical stress from periodic stretching. Exp Cell Res *268*, 104-114.

Higgs, H.N. (2005). Formin proteins: a domain-based approach. Trends Biochem Sci *30*, 342-353.

Higgs, H.N., and Pollard, T.D. (2000). Activation by Cdc42 and PIP(2) of Wiskott-Aldrich syndrome protein (WASp) stimulates actin nucleation by Arp2/3 complex. J Cell Biol *150*, 1311-1320.

Hirata, H., Tatsumi, H., and Sokabe, M. (2008). Mechanical forces facilitate actin polymerization at focal adhesions in a zyxin-dependent manner. J Cell Sci *121*, 2795-2804.

Holmes, K.C., Popp, D., Gebhard, W., and Kabsch, W. (1990). Atomic model of the actin filament. Nature *347*, 44-49.

Howard, J. (2001). Mechanics of Motor Proteins and the Cytoskeleton (Sinauer Associates Inc.).

Humphrey, W., Dalke, A., and Schulten, K. (1996). VMD-visual molecular dynamics. J Mol Graph *14*, 33-38.

Kabsch, W., Mannherz, H.G., Suck, D., Pai, E.F., and Holmes, K.C. (1990). Atomic structure of the actin:DNase I complex. Nature *347*, 37-44.

Kaunas, R., Nguyen, P., Usami, S., and Chien, S. (2005). Cooperative effects of Rho and mechanical stretch on stress fiber organization. Proc Natl Acad Sci U S A *102*, 15895-15900.

Kishino, A., and Yanagida, T. (1988). Force measurements by micromanipulation of a single actin filament by glass needles. Nature *334*, 74-76.

Kolega, J. (1986). Effects of mechanical tension on protrusive activity and microfilament and intermediate filament organization in an epidermal epithelium moving in culture. J Cell Biol *102*, 1400-1411.

Kong, F., Garcia, A.J., Mould, A.P., Humphries, M.J., and Zhu, C. (2009). Demonstration of catch bonds between an integrin and its ligand. J Cell Biol *185*, 1275-1284.

Kovar, D.R. (2006). Molecular details of formin-mediated actin assembly. Curr Opin Cell Biol *18*, 11-17.

Kovar, D.R., and Pollard, T.D. (2004). Insertional assembly of actin filament barbed ends in association with formins produces piconewton forces. Proc Natl Acad Sci U S A *101*, 14725-14730.

Laing, N.G., Dye, D.E., Wallgren-Pettersson, C., Richard, G., Monnier, N., Lillis, S., Winder, T.L., Lochmuller, H., Graziano, C., Mitrani-Rosenbaum, S.*, et al.* (2009). Mutations and polymorphisms of the skeletal muscle alpha-actin gene (ACTA1). Hum Mutat *30*, 1267-1277.

Li, F., and Higgs, H.N. (2003). The mouse Formin mDia1 is a potent actin nucleation factor regulated by autoinhibition. Curr Biol *13*, 1335-1340.

Li, F., and Higgs, H.N. (2005). Dissecting requirements for auto-inhibition of actin nucleation by the formin, mDia1. J Biol Chem *280*, 6986-6992.

Lou, J., and Zhu, C. (2007). A structure-based sliding-rebinding mechanism for catch bonds. Biophys J *92*, 1471-1485.

MacKerell, A., Jr., Bashford, D., Bellott, M., Dunbrack, R.L.J., Evanseck, J., Field, M.J., Fischer, S., Gao, J., Guo, H., Ha, S.*, et al.* (1998). All-atom empirical potential for molecular modeling and dynamics Studies of proteins. J Phys Chem B *102*, 3586-3616.

Maekawa, M., Ishizaki, T., Boku, S., Watanabe, N., Fujita, A., Iwamatsu, A., Obinata, T., Ohashi, K., Mizuno, K., and Narumiya, S. (1999). Signaling from Rho to the actin cytoskeleton through protein kinases ROCK and LIM-kinase. Science *285*, 895-898.

Marshall, B.T., Long, M., Piper, J.W., Yago, T., McEver, R.P., and Zhu, C. (2003). Direct observation of catch bonds involving cell-adhesion molecules. Nature *423*, 190-193.

Marshall, B.T., Sarangapani, K.K., Wu, J., Lawrence, M.B., McEver, R.P., and Zhu, C. (2006). Measuring molecular elasticity by atomic force microscope cantilever fluctuations. Biophys J *90*, 681-692.

McCue, S., Noria, S., and Langille, B.L. (2004). Shear-induced reorganization of endothelial cell cytoskeleton and adhesion complexes. Trends Cardiovasc Med *14*, 143-151.

Narumiya, S., Ishizaki, T., and Watanabe, N. (1997). Rho effectors and reorganization of actin cytoskeleton. FEBS Lett *410*, 68-72.

Nobes, C.D., and Hall, A. (1995). Rho, rac, and cdc42 GTPases regulate the assembly of multimolecular focal complexes associated with actin stress fibers, lamellipodia, and filopodia. Cell *81*, 53-62.

Oda, T., Iwasa, M., Aihara, T., Maeda, Y., and Narita, A. (2009). The nature of the globular- to fibrous-actin transition. Nature *457*, 441-445.

Otomo, T., Tomchick, D.R., Otomo, C., Panchal, S.C., Machius, M., and Rosen, M.K. (2005). Structural basis of actin filament nucleation and processive capping by a formin homology 2 domain. Nature *433*, 488-494.

Otterbein, L.R., Graceffa, P., and Dominguez, R. (2001). The crystal structure of uncomplexed actin in the ADP state. Science *293*, 708-711.

Parekh, S.H., Chaudhuri, O., Theriot, J.A., and Fletcher, D.A. (2005). Loading history determines the velocity of actin-network growth. Nat Cell Biol *7*, 1219-1223.

Paul, A.S., and Pollard, T.D. (2008). The role of the FH1 domain and profilin in formin-mediated actin-filament elongation and nucleation. Curr Biol *18*, 9-19.

Paul, A.S., and Pollard, T.D. (2009). Review of the mechanism of processive actin filament elongation by formins. Cell Motil Cytoskeleton *66*, 606-617.

Phillips, J.C., Braun, R., Wang, W., Gumbart, J., Tajkhorshid, E., Villa, E., Chipot, C., Skeel, R.D., Kale, L., and Schulten, K. (2005). Scalable molecular dynamics with NAMD. J Comput Chem *26*, 1781-1802.

Pollard, T.D. (1986). Rate constants for the reactions of ATP- and ADP-actin with the ends of actin filaments. J Cell Biol *103*, 2747-2754.

Pollard, T.D., and Borisy, G.G. (2003). Cellular motility driven by assembly and disassembly of actin filaments. Cell *112*, 453-465.

Pollard, T.D., and Cooper, J.A. (2009). Actin, a central player in cell shape and movement. Science *326*, 1208-1212.

Pring, M., Evangelista, M., Boone, C., Yang, C., and Zigmond, S.H. (2003). Mechanism of formin-induced nucleation of actin filaments. Biochemistry *42*, 486-496.

Pruyne, D., Evangelista, M., Yang, C., Bi, E., Zigmond, S., Bretscher, A., and Boone, C. (2002). Role of formins in actin assembly: nucleation and barbed-end association. Science *297*, 612-615.

Sanoudou, D., and Beggs, A.H. (2001). Clinical and genetic heterogeneity in nemaline myopathy--a disease of skeletal muscle thin filaments. Trends Mol Med *7*, 362-368.

Sept, D., and McCammon, J.A. (2001). Thermodynamics and kinetics of actin filament nucleation. Biophys J *81*, 667-674.

Soeno, Y., Abe, H., Kimura, S., Maruyama, K., and Obinata, T. (1998). Generation of functional beta-actinin (CapZ) in an E. coli expression system. J Muscle Res Cell Motil *19*, 639-646.

Sung, H.J., Yee, A., Eskin, S.G., and McIntire, L.V. (2007). Cyclic strain and motion control produce opposite oxidative responses in two human endothelial cell types. Am J Physiol Cell Physiol *293*, C87-94.

Takagi, Y., Homsher, E.E., Goldman, Y.E., and Shuman, H. (2006). Force generation in single conventional actomyosin complexes under high dynamic load. Biophys J *90*, 1295-1307.

Tsuda, Y., Yasutake, H., Ishijima, A., and Yanagida, T. (1996). Torsional rigidity of single actin filaments and actin-actin bond breaking force under torsion measured directly by in vitro micromanipulation. Proc Natl Acad Sci U S A *93*, 12937-12942.

Vinay Kumar, Abul K. Abbas, Nelson Fasto, and Aster, J.C. (2010). Robbins and Cotran Pathologic Basis of Disease, 8 edn (philadelphia, Saunders, Elsevier).

Watanabe, N., Kato, T., Fujita, A., Ishizaki, T., and Narumiya, S. (1999). Cooperation between mDia1 and ROCK in Rho-induced actin reorganization. Nat Cell Biol *1*, 136-143.

Wu, J., Fang, Y., Yang, D., and Zhu, C. (2005). Thermo-mechanical responses of a surface-coupled AFM cantilever. J Biomech Eng *127*, 1208-1215.

Xu, Y., Moseley, J.B., Sagot, I., Poy, F., Pellman, D., Goode, B.L., and Eck, M.J. (2004). Crystal structures of a Formin Homology-2 domain reveal a tethered dimer architecture. Cell *116*, 711-723.

Yago, T., Lou, J., Wu, T., Yang, J., Miner, J.J., Coburn, L., Lopez, J.A., Cruz, M.A., Dong, J.F., McIntire, L.V.*, et al.* (2008). Platelet glycoprotein Ibalpha forms catch bonds with human WT vWF but not with type 2B von Willebrand disease vWF. J Clin Invest *118*, 3195-3207.

Yakovenko, O., Sharma, S., Forero, M., Tchesnokova, V., Aprikian, P., Kidd, B., Mach, A., Vogel, V., Sokurenko, E., and Thomas, W.E. (2008). FimH forms catch bonds that are enhanced by mechanical force due to allosteric regulation. J Biol Chem *283*, 11596-11605.

Zigmond, S.H. (2004). Formin-induced nucleation of actin filaments. Curr Opin Cell Biol *16*, 99-105.

Zigmond, S.H., Evangelista, M., Boone, C., Yang, C., Dar, A.C., Sicheri, F., Forkey, J., and Pring, M. (2003). Formin leaky cap allows elongation in the presence of tight capping proteins. Curr Biol *13*, 1820-1823.